Dalton Transactions

Accepted Manuscript

ROYAL SOCIETY OF CHEMISTRY

www.rsc.org/dalton

Reviewer(s)' Comments to Author:

Referee: 1

Comments to the Author

DT-ART-01-2015-000022

Structural investigation of the A-site vacancy in Scheelites and the luminescence behaviors of two continuous solid solutions A1-1.5xEux□0.5xWO4 and A0.64-0.5yEu0.24Liy□0.12-0.5yWO4 (A = Ca, Sr; □ = vacancy)

The authors report on the synthesis and characterization of a series of compounds with A1-1.5xEux□0.5xWO4 and A0.64-0.5yEu0.24Liy□0.12-0.5yWO4 (A = Ca, Sr; □ = vacancy) chemical composition. These systems crystallize in Scheelite structure type and have received a great deal of interest due to their optical properties. The authors have proposed two possible mechanisms for the charge balance during the substitution of the A2+ ions by trivalent Eu3+, namely (i) cation site vacancy and (ii) interstitial addition of O2- ions.

Their detailed powder X-ray diffraction analyses along with their spectroscopic studies support the former mechanism. Although powder X-ray diffraction is not the best way to study oxygen occupancies and neutron data are needed for more accurate investigation, the provided complementary crystallographic and spectroscopic data are in accordance with their conclusion. The manuscript is written very well and provides many useful details about the structural and optical properties of the title phases.

In conclusion, I think that this article will be beneficial for the solid-state chemistry community and I recommend its publication in Dalton Transactions.

Response: Thanks very much for the positive comments.

Referee: 2

Comments to the Author

The manuscript reports on successful syntesis, structural characterization and luminescent properties of four scheelite-based Eu-doped solid solutions. The manuscript suits Dalton Transactions well and deserves to be published after taking into account the following comments:

Please, specify the impurity phases which appear upon exceeding the alleged Eu and Li doping limits.

Response: An additional figure was presented in ESI as Fig. S1. For the cases of Eu^{3+}/Li^{+} co-doped samples, we did not observe any impurity.

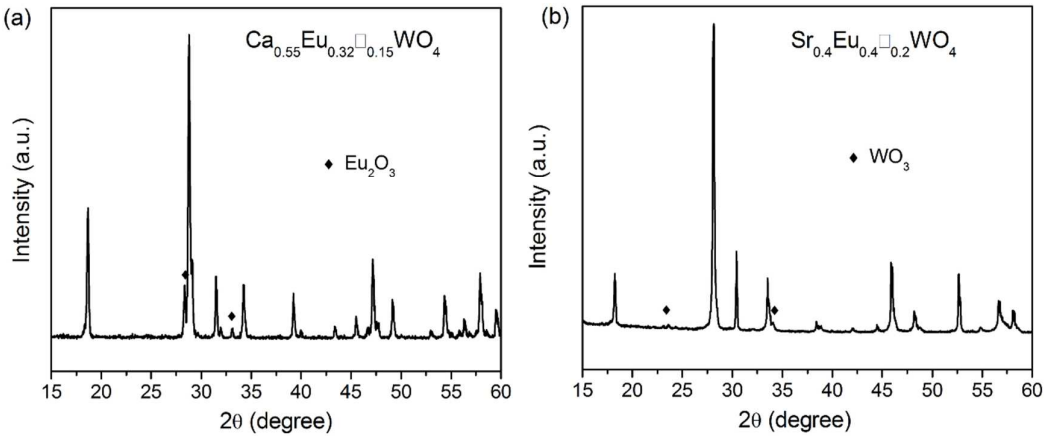

Fig. S1 XRD patterns for "$Ca_{0.55}Eu_{0.32}\square_{0.15}WO_4$" and "$Sr_{0.4}Eu_{0.4}\square_{0.2}WO_4$" samples prepared by high temperature solid state reactions. Other than the major phase of Scheelite, minor impurity peaks appear as marked in above figures, either belong to Eu_2O_3 or WO_3. There supposed to be other impurities, however, probably their diffraction peaks are overlapped with the major phase, it is hard to identify all of them. Nevertheless, our experiments show that the assumed compositions "$Ca_{0.55}Eu_{0.32}\square_{0.15}WO_4$" and "$Sr_{0.4}Eu_{0.4}\square_{0.2}WO_4$" cannot be annealed to be phase-pure.

The variation of the unit cell parameters is not well explained. The interesting observation is the different trends in the unit cell volume upon increasing x for the SEW and CEW solid solutions. Authors attribute it to the attraction of the oxygen ions by Eu3+ apart from W6+, resulting in the increase of W6+-O bond distance. However, they overlook the fact that for the CELW and SELW solid solutions such increase does not occur. How to explain this discrepancy?

Response: The difference trends in the unit cell change is indeed interesting. For example, when we used a smaller cation Eu^{3+} to replace a relatively larger Ca^{2+}, it gave an expansion of cell volume. We attribute this to the difference oxidation states between these two cations, where Eu^{3+} has a large attraction effect to oxygen. In the cases of **SEW** and **SELW**, it is the same. The W-O bond distance in **SEW**, **SELW** also shows an increasing tendency as shown in Fig. 4. However, the changes in **CELW** are not obvious. We explained this as below (it is inserted as the last paragraph of the structure refinement section).

"In $Ca_{0.64-0.5y}Eu_{0.24}Li_y\square_{0.12-0.5y}WO_4$ ($0 \le y \le 0.24$), the incorporation of Li^{+} leads to a moderate shrinkage of the unit cell volume (-1.6 Vol.%), comparing to the minor change in **CEW** (+0.6 Vol.%). The *A*-O and W-O bond distances almost kept constant. We speculate the real changes in bond distance are probably not significant enough and close to the accuracy of powder XRD refinements."

The effect of the local symmetry distortion of the Eu3+ coordination environment calls for more extended explanation. The refined crystal structures suggest the S4 symmetry, but what is the exact reason for deviation? What is the meaning of "different valance between Eu3+ and A2+" (balance? valence?)? How exactly the polarizability of the WO4 groups is involved in this local distortions?

Please, explain the appearance of the 5D0 → 7F0 peak in the spectra of CEW and SEW. This peak is forbidden by tetragonal symmetry and must be absent.

Response: About the site symmetry deviation issue of Eu^{3+}, we referred to a previous report (Chem. Mater. 2008, 20, 6060-6067, synthesis and optimum luminescence of $CaWO_4$-based red phosphors with codoping of Eu^{3+} and Na^{+}). Accordingly we revised our maintext as shown below.

"For **SEW** and **CEW**, the *R*/*O* values are around 9.3 and 9.6 (see Fig. 7), respectively, which is a strong evidence that Eu^{3+} ions mainly occupy the lattice site without inversion symmetry.

It is well known that both of $CaWO_4$ and $SrWO_4$ crystallize in the tetragonal Scheelite structure with the space group of $I4_1/a$, in which the *A* cation is coordinated by eight oxygen atoms with the S_4 point symmetry (no inversion center). In fact, it is reported in literature that the aliovalent Eu^{3+}-to-A^{2+} doping (together with the presence of the *A*-site vacancies in our case) could induce a local deviation of the site symmetry of Eu^{3+} from S_4 symmetry.[25] This is proved by the presence of very weak $^5D_0 \rightarrow {}^7F_0$ emission at 581 nm since this emission is only allowed for C_s, C_n, C_{nv} site symmetry.[37] Of course, the deviation of the S_4 symmetry of Eu^{3+} was also confirmed by the large *R*/*O* values."

25 Y. G. Su, L. P. Li, G. S. Li, *Chem. Mater.* 2008**, 20**, 6060-6067.

37 G. Blass, A. Bril, *Philips Res. Rep.* 1966, **2**, 268.

We hope our explanation would be accepted.

It seems that the authors relate the saturation of luminescence with the concentration of the A-site vacancies. It contradicts with the recent finding of similar saturation in the CaGd2(1−x)Eu2x(BO4)4 (B = Mo, W) solid solutions where the saturation occurs upon increasing the Eu content while maintaining the constant concentration of the A-site vacancies (see Chem. Mater. 2013, 25, 4387−4395). This discrepancy should be mentioned and discussed.

Response: In both our cases and $CaGd_{2(1-x)}Eu_{2x}(BO_4)_4$ (B = Mo, W), similar saturation phenomena were observed. They are not conflict. With the increasing of the activator content, the emission intensity does not increase but becomes saturated. It is an indication of the non-radiative cross-relaxation, which can occur in various routes, like between excited and unexcited Eu^{3+} ions,

or from excited Eu^{3+}/WO_4 to defects. In $CaGd_{2(1-x)}Eu_{2x}(BO_4)_4$, the emission saturation (or we can say the absence of concentration quenching effect) was interpreted to be due to the large Eu-Eu distance. In our cases of **SEW** and **CEW**, the *A*-site vacancies would increase along with the increase of Eu^{3+} content, therefore behavior as additional energy consuming centers. Accordingly, we present an additional paragraph in the maintext as shown below.

"Recently, a structure and luminescence study on $CaGd_{2(1-x)}Eu_{2x}(BO_4)_4$ (B = Mo, W) shows a similar phenomenon of luminescence saturation at $x = 0.5$, which means 25% of *A*-sites are occupied by Eu^{3+}.[38] The high concentration of activators for emission saturation is due to a relatively large Eu-Eu distances in Scheelite structure. Here in our cases of **CEW** and **SEW**, the increase of the Eu^{3+} also results in an increase of *A*-site vacancies, therefore the saturation occurs at a lower level of Eu^{3+} content ($x = 0.2$)."

38 V. A. Morozov, A. Bertha, K. W. Meert, S. Van Rompaey, D. Batuk, G. T. Martinez, S. Van Aert, P. F. Smet, M. V. Raskina, D. Poelman, A. M. Abakumov, J. Hadermann, *Chem. Mater.* 2013, **25**, 4387-4395

Some technical comments:

1) "it is relatively difficult to simply replace one A2+ by one Eu3+ ion .... without additional way of charge balance." – this sentence looks odd because it actually says that it is difficult, BUT possible to do such replacement and violate the charge balance.

2) "exhibit modulated superstructures in (3+1)-, (3+2)-, (3+1)- and (3+1)-dimensional super space groups, respectively" – please, correct as " exhibit modulated superstructures in (3+1)- and (3+2)-dimensional super space groups."

3) "Scheelite compounds crystallize in the tetrahedral symmetry" – tetragonal, not tetrahedral.

4) "According to the Rietveld refinements, we confirmed the type II mechanism" – according to the definitions given in the manuscript, it should be the mechanism I.

5) Correct the author's names in the reference 33.

6) The manuscript is well written, but some language mistakes are still present. Please, let it be checked by a native speaker or through one of the available services

Response: Thanks. Suggested changes are done. We went through the manuscript very carefully, and did our best to polish the language usage.

ARTICLE Dalton Transactions

Cite this: DOI: 10.1039/x0xx00000x

Received ooth January 2012,
Accepted ooth January 2012

DOI: 10.1039/x0xx00000x

www.rsc.org/

Structural investigation of the *A*-site vacancy in Scheelites and the luminescence behaviors of two continuous solid solutions $A_{1-1.5x}Eu_x\square_{0.5x}WO_4$ and $A_{0.64-0.5y}Eu_{0.24}Li_y\square_{0.12-0.5y}WO_4$ (*A* = Ca, Sr; □ = vacancy)

Pengfei Jiang,[a] Wenliang Gao,[a] Rihong Cong,[a*] and Tao Yang[a*]

Scheelite compounds with Eu^{3+} substitution are well-known red-phosphors. We prepared and performed a detailed structural characterizations on $A_{1-1.5x}Eu_x\square_{0.5x}WO_4$ and $A_{0.64-0.5y}Eu_{0.24}Li_y\square_{0.12-0.5y}WO_4$ (*A* = Ca, Sr; □ = vacancy) to confirm the *A*-site vacancy mechanism for charge balance when bivalent A cations were substituted by Eu^{3+}. All compounds crystallize in $I4_1/a$ with a disordering arrangement of A^{2+}, Eu^{3+}, □ at *A*-site. The title compounds are all good red phosphors with high R/O ratio (~10), indicating that Eu^{3+} locates at a significantly distorted cavity. $A_{1-1.5x}Eu_x\square_{0.5x}WO_4$ shows a saturation phenomenon at a high doping level, x = 0.20. With the incorporation of Li^+, the emission intensity was generally enhanced comparing to the Li^+-free samples, moreover, the increasing of Li^+ content reduce the content of vacancy, resulting in an further increasing of the luminescent intensity.

Introduction

Scheelite is a large family with the composition ABO_4. *A*- and *B*-cations can be different elements with various valence states. For instance, $K^+Re^{7+}O_4$[1] and $Ag^+I^{7+}O_4$,[2] $Cd^{2+}(Mo/W)^{6+}O_4$[3-4] and $Pb^{2+}(Mo/W)^{6+}O_4$,[5] $Y^{3+}(Nb/V)^{5+}O_4$,[6-7] $Zr^{4+}Ge^{4+}O_4$[8] all possess the Scheelite-type structure, where *A*-cations are 8-fold coordinated and *B*-cations are 4-fold coordinated (see Fig. 1a). Compounds with Scheelite-type structure have been studied as the potential laser materials and oxygen ion conductors for many years.[9-14] For example, $M_{0.5}Ln_{0.5}BO_4$ (*M* = Li, Na, or K; *Ln* = lanthanides; *B* = W or Mo) single crystals are used as potential self-doubling solid-state laser host materials;[9-11] $PbWO_4$:Ln^{3+} (*Ln* = La, Pr, Sm or Tb) are good oxygen ion conductors.[13-14] In the past decade, the potential of Scheelite compounds as host materials for white-LEDs were extensively explored, like Eu^{3+} activated (Ca/Sr)BO_4 (*B* = W or Mo) are efficient LED red phosphors.[15-19] Moreover, great efforts are also devoted to the synthetic methods in order to improve their luminescent performance. For example, in addition to the conventional high temperature solid-state reaction, other techniques like co-precipitation, combustion and hydrothermal methods were also employed, which can efficiently modify the crystal-size distribution and micro-morphology of phosphors.[20-25]

From the structural point of view, there should be a charge balance mechanism in order to replace one A^{2+} by one Eu^{3+} ion (a commonly used luminescent activator). One may think that the interstitial oxygen mechanism is an option (i.e. $A_{1-x}Eu_xWO_{4+0.5x}$). Such a mechanism could be applicable in Pb^{2+}-Scheelite, but not commonly seen in Sr- or Ca-based Scheelite compounds. Actually, there are two additional methods to maintain the electrical neutrality during the Eu^{3+}-substitution. For example, A^{2+} in ABO_4 (*A* = Ca or Sr, *B* = W or Mo) can be successfully substituted by a co-doping of Eu^{3+}/M^+ (*M* = Li, Na, or K), which in fact could greatly enhance the luminescent intensity.[15, 25-27] Besides, one has proved that the Scheelite structure allows the existence of *A*-site vacancies, i.e. $M_{2/7}Gd_{4/7}\square_{1/7}MoO_4$ (*M* = Li^+ or Na^+; □ = *A*-site vacancies), therefore, the occurrence of cation vacancies along with Eu^{3+} doping is another way of charge balance. Moreover, there are two representative examples, $R_2\square B_3O_{12}$ (*R* = rare earth, Y, or Bi, *B* = W or Mo, □ = vacancy), showing an ordering arrangement between *A*-site cations and vacancies (see Figs. 1b and 1c).[28-30]

Here, partial solid solutions of $Sr_{1-1.5x}Eu_x\square_{0.5x}WO_4$ ($0.04 \le x \le 0.36$) (denoted as **SEW**), $Ca_{1-1.5x}Eu_x\square_{0.5x}WO_4$ ($0.04 \le x \le 0.24$) (**CEW**), and $A_{0.64-0.5y}Eu_{0.24}Li_y\square_{0.12-0.5y}WO_4$ (*A* = Ca or Sr; $0 \le y \le 0.24$) (**CELW and SELW**) were prepared by high temperature solid state reactions. It is interesting to prepare Scheelite-type phosphors with continuously variable concentrations of both Eu^{3+} and *A*-site vacancies, and an investigation on the influences of Eu^{3+} and vacancy contents on the photoluminescence were performed in detail.

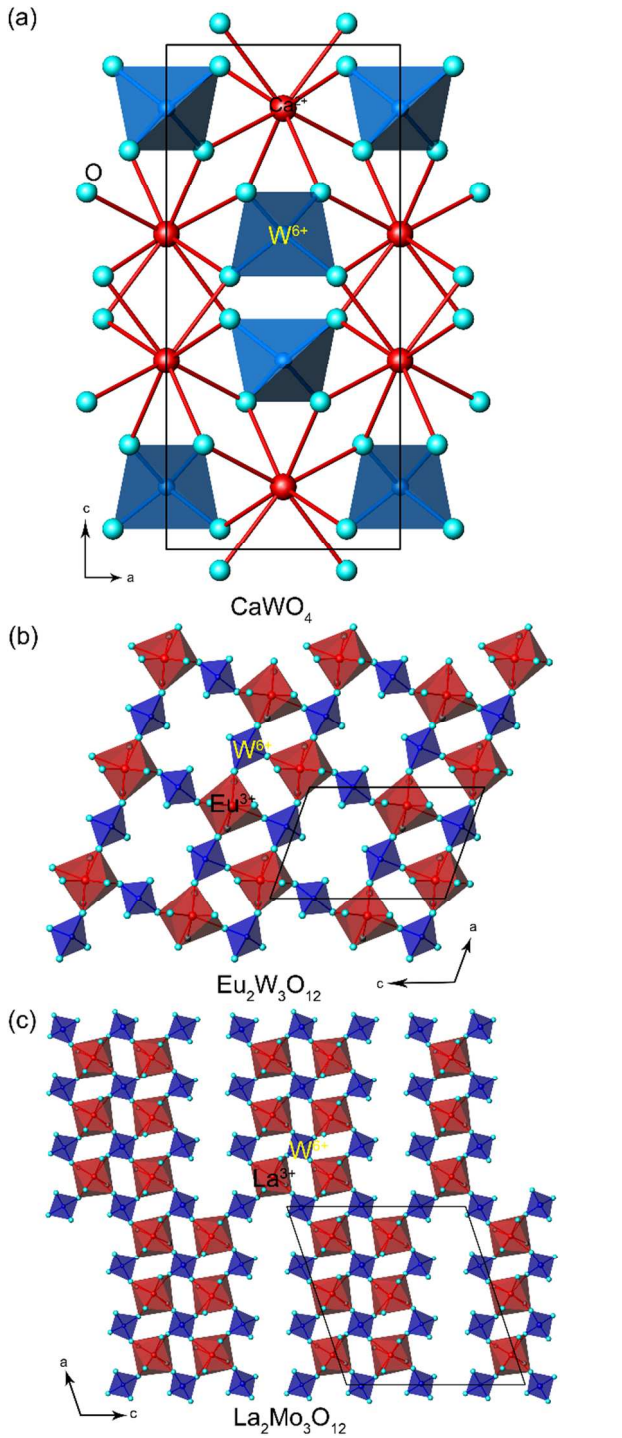

Fig. 1 (a) An example of tetragonal Scheelite structure; two representatives showing vacancy-ordered Scheelite structure (b) $Eu_2W_3O_{12}$ and (c) $La_2Mo_3O_{12}$.

Experimental

The solid solutions $Sr_{1-1.5x}Eu_x\square_{0.5x}WO_4$ ($0.04 \leq x \leq 0.36$) and $Ca_{1-1.5x}Eu_x\square_{0.5x}WO_4$ ($0.04 \leq x \leq 0.24$) were prepared by high temperature solid-state reactions at 1100 ºC and 1200 ºC, respectively. $SrCO_3$ (99.9%), $CaCO_3$ (99.9%), Eu_2O_3 (99.99%), WO_3 (99.5%) and Li_2CO_3 (99.99%) were used as the starting materials. First, the raw materials except Li_2CO_3 were pre-heated at 400 ºC for 10 hours to remove the absorbed moisture. Then, stoichiometric amounts of the reagents were ground in an agate mortar, and heated at 800 ºC for 10 hours to decompose the carbonate. After an extensive re-grounding, the samples were re-heated at the final reaction temperature for 15 hours. For the syntheses of lithium co-doped samples, $A_{0.64-0.5y}Eu_{0.24}Li_y\square_{0.12-0.5y}WO_4$ (A = Ca or Sr; $0.04 \leq y \leq 0.24$), the annealing temperature was 950 ºC (A = Ca) and 900 ºC (A = Sr), respectively.

Powder X-ray diffraction (XRD) analysis was carried on a PANalytical Empyrean diffractometer equipped with a PIXcel 3D detector (Cu Kα radiation). The operation voltage and current were 40 kV and 40 mA, respectively. Rietveld refinements were performed using the software package TOPAS.[31] Photoluminescence spectra were measured on a Hitachi F4600 fluorescence spectrometer at room temperature. The voltage of Xe lamp was fixed at 700 V, and both of the input and output slits were selected to be 1 nm. The emission intensities are calculated from the integral of the corresponding peaks.

Results and discussion

Phase purity

$Sr_{1-1.5x}Eu_x\square_{0.5x}WO_4$ ($0.04 \leq x \leq 0.36$), $Ca_{1-1.5x}Eu_x\square_{0.5x}WO_4$, ($0.04 \leq x \leq 0.24$), and $A_{0.64-0.5y}Eu_{0.24}Li_y\square_{0.12-0.5y}WO_4$ ($0 \leq y \leq 0.24$) (A = Ca or Sr) phosphors were obtained as white powder. In order to clarify the purity of the samples, powder XRD for all specimens were conducted (see Fig. 2). It can be seen that all the diffracting peaks of samples are consistent with the Scheelite structure, and no impurity peak was observed. In addition, it is obvious that the reflection peaks for Eu^{3+} and Eu^{3+}/Li^+-doped $SrWO_4$ samples shift to higher angles, indicating the significant shrinkage of the unit cell. This is a strong evidence of the successful substitution. For those doped $CaWO_4$ samples, the peak shifting is not that obvious, nevertheless, the change of the lattice parameters can be determined by Le Bail refinements on their powder XRD patterns. These changes are linearly in accordance with the doping level as shown in Fig. 3. Therefore it is conclusive that our syntheses of Eu^{3+} and Eu^{3+}/Li^+ incorporated AWO_4 (A = Ca, Sr) were successful, and the doping did not make any significant change to the crystal structure. Further increasing the doping level of Eu^{3+}, impurity peaks would appear (see Fig. S1 in the electronic supplementary information, ESI). It is interesting to observe that the Eu^{3+}-doping of $Ca_{1-1.5x}Eu_x\square_{0.5x}WO_4$ leads to an observable expansion of the unit cell volume (about 0.6%), which will be explained in later section.

Doping mechanism and structure refinements

In Scheelite structure, Ca^{2+}/Sr^{2+} ion occupies the 8-fold coordination cavity, forming a distorted CaO_8/SrO_8 polyhedra. Whereas W^{6+} ion occupies the 4-fold coordination site, and all

the WO_4^{2-} tetrahedral are isolated by the *A*-site cations (see Fig. 1a). As an extensively investigated phosphor host, it is very

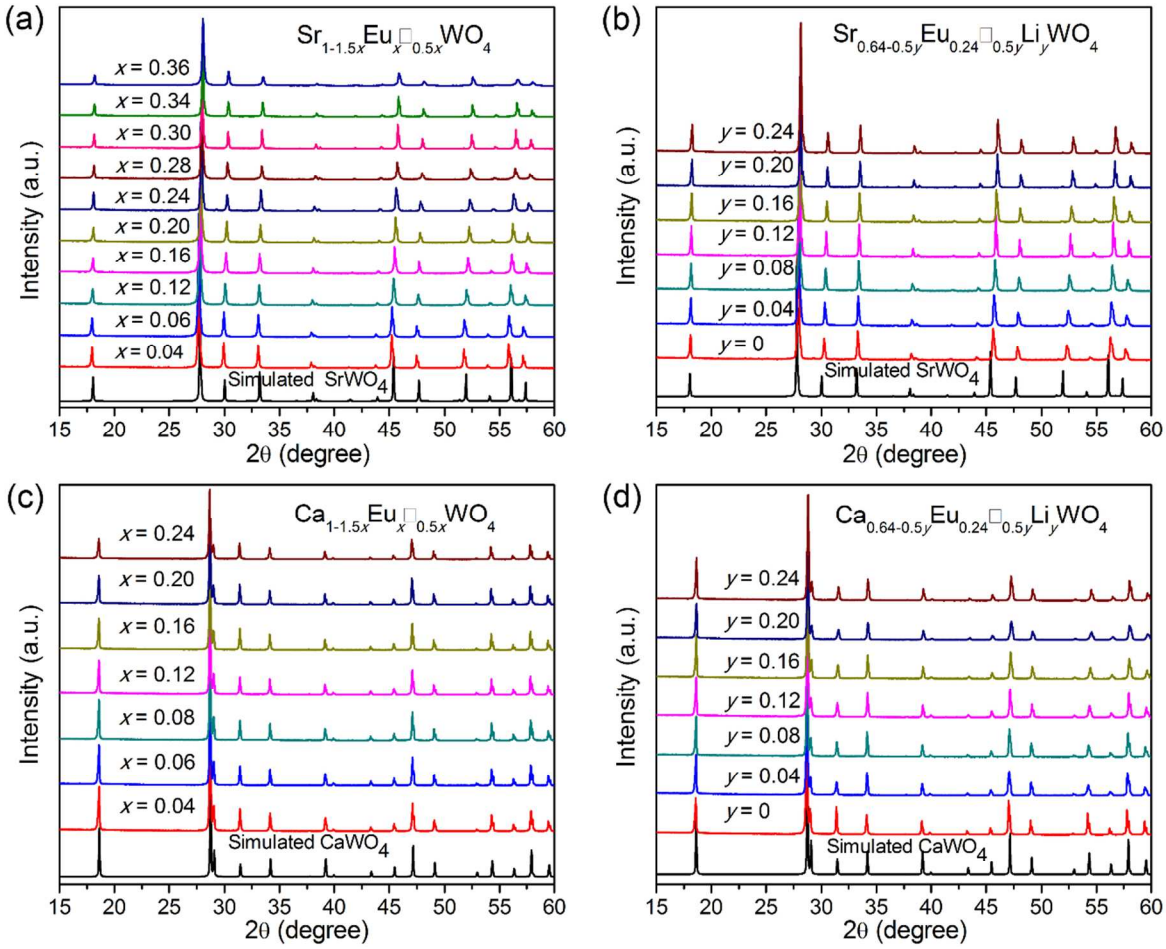

Fig. 2 XRD patterns for Eu^{3+}-doped and Eu^{3+}/Li^+-co-doped Scheelite compounds. Simulated patterns for $SrWO_4$ and $CaWO_4$ based on structures are shown as reference.

important to figure out the aliovalent doping mechanism for the rare-earth cations substitution. For example, replacing a bivalent cation A^{2+} by a trivalent Eu^{3+} would lead to an additional positive charge. Two possible mechanisms to keep the charge neutrality include creating *A*-site vacancies or taking interstitial oxygen atoms, which can be expressed as $3Sr_{Sr} \rightarrow 2Eu_{Sr}^{\cdot} + V_{Sr}''$ (type I), forming $Sr_{1-1.5x}Eu_x\square_{0.5x}WO_4$ and $2Sr_{Sr} \rightarrow 2Eu_{Sr}^{\cdot} + O_i''$ (type II), forming $Sr_{1-x}Eu_xWO_{4+x/2}$, respectively.

We notice that the type II mechanism was reported in $Pb_{1-x}Ln_xWO_{4+x}$ (*Ln* = La, Pr, Sm, Tb, $x \leq 0.4$), which in fact exhibits a substantial oxygen ion conductivity.[12-14] Here in our study, we failed to obtain pure powder samples with the formula $Sr_{0.92}Eu_{0.08}WO_{4.04}$ and $Ca_{0.90}Eu_{0.10}WO_{4.05}$ (see Fig. S2 in ESI), which are two representative samples in literature, showing strongest emission intensities in $Sr_{1-x}Eu_xWO_4$ and $Ca_{1-x}Eu_xWO_4$, respectively.[16, 22] Our experimental results suggest that Ca^{2+}- and Sr^{2+}-Scheelite compounds prefer the type I mechanism for charge balance. No interstitial oxygen atoms are allowed in the title systems, where indeed no ionic conductivity was observed at high temperatures for a selected sample "$Ca_{0.7}Eu_{0.22}WO_{4.03}$" (see Fig. S3 in ESI). In other words, *A*-site vacancies are artificially produced as charge compensations in the **CEW** and **SEW** systems. In ***A*ELW** systems, both *A*-site vacancies and Li^+ served as charge compensations.

Typically, Scheelite compounds crystallize in the tetragonal symmetry, while there exist Scheelite-type compounds with 1/3 A-site vacancies showing a distorted monoclinic symmetry, i.e. $Eu_2\square W_3O_{12}$ crystallizes in the space group *C*2/*c*.[32] Moreover, $Ag_{1/8}Pr_{5/8}\square_{1/4}MoO_4$, $Na_{2/7}Gd_{4/7}\square_{1/7}MoO_4$, $CaEu_2\square(BO_4)_4$ (*B* = Mo and W) and $Na_xEu_{(2-x)/3}\square_{(1-2x)/3}MoO_4$ ($x \leq 0.25$) which all have less than 1/3 *A*-site vacancies and therefore exhibit modulated super-structures in (3+1)- and (3+2)-dimensional super space groups, respectively.[33-36] An incommensurately modulated structure usually can be verified by additional satellite reflections at the lower angle part of XRD. Herein, the *A*-site vacancy concentrations reach the maxima of 0.18 and 0.12 in **CEW** and **SEW**, respectively, without showing any satellite reflection in the lower angle neither a monoclinic distortion was observed.

Rietveld refinements for selected samples were therefore performed using the tetragonal Scheelite structure as the

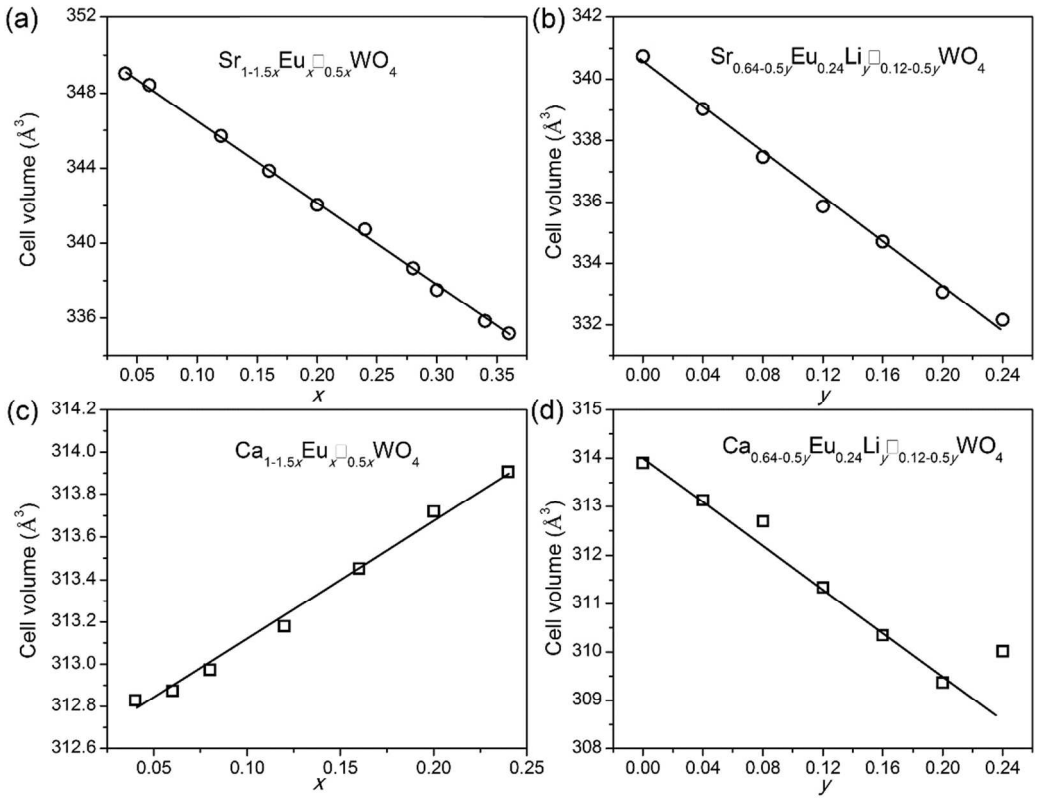

Fig. 3 Calculated cell volumes by Le Bail fitting on whole XRD patterns of title compounds.

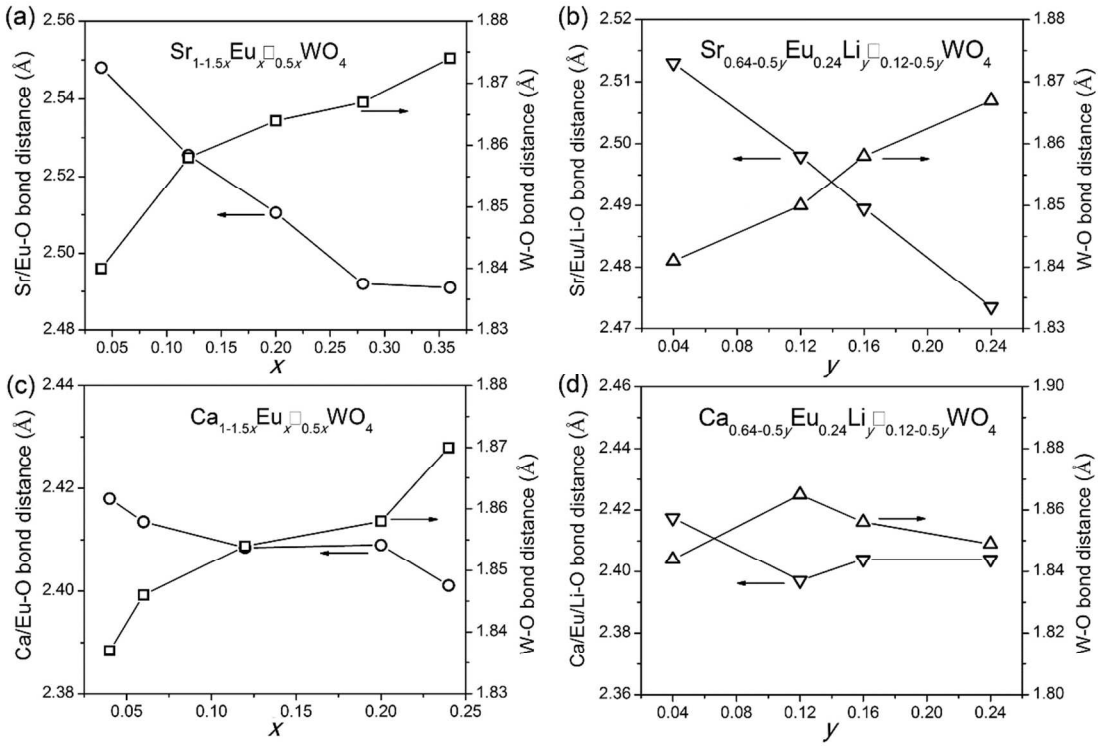

Fig. 4 Average bond distances of A-O and W-O for selected samples.

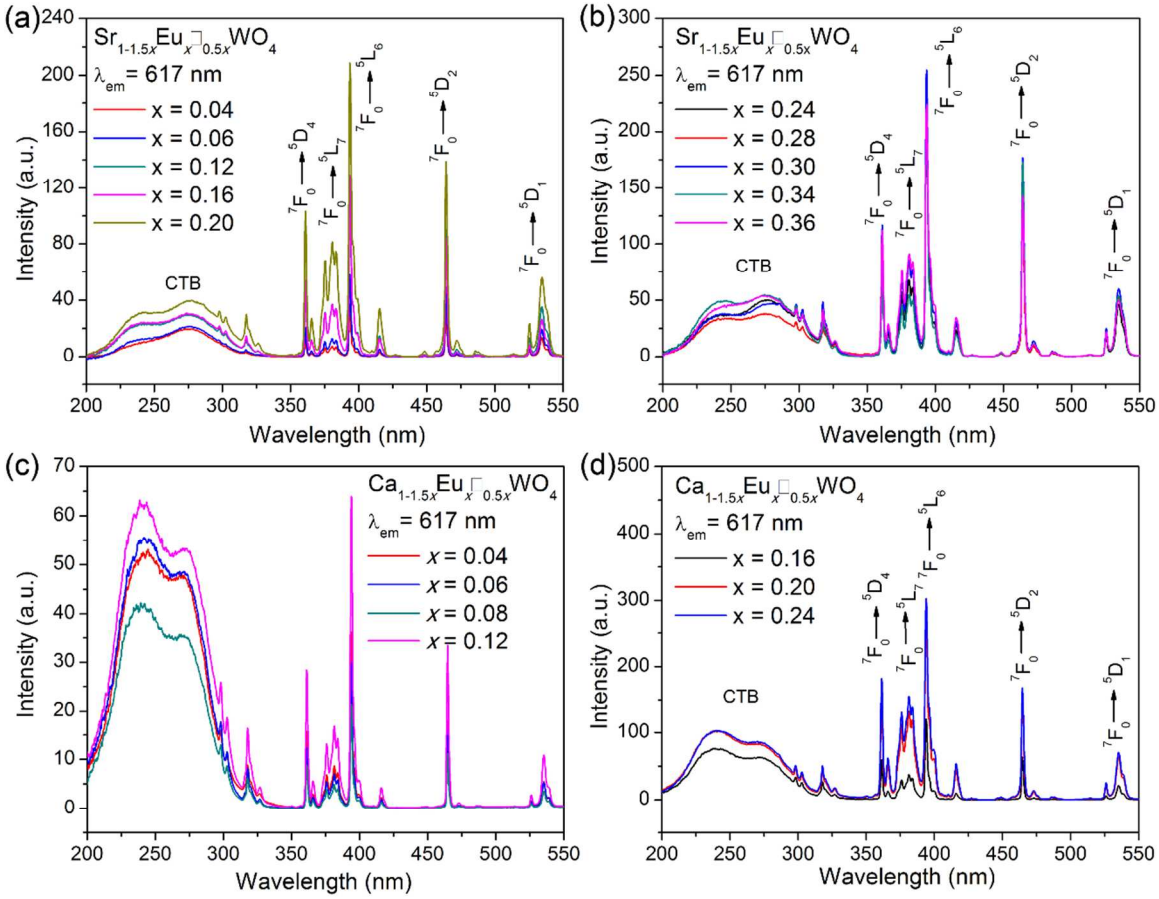

Fig. 5 Excitation spectra by monitoring the emission at 617 nm for Eu^{3+}-doped $SrWO_4$ and $CaWO_4$ samples.

starting model, where Li^+, A^{2+} and Eu^{3+} cations are randomly distributed. In **CEW** and **SEW** systems, the occupy factor of Eu^{3+} was set as x, and the occupancy factor for Ca^{2+}/Sr^{2+} was refined freely. With such a constraint, the occupancy factor for Ca^{2+}/Sr^{2+} converged to a value close to 1-1.5x within an acceptable error. In other words, the A-site cavities are not completely occupied by Ca^{2+}/Sr^{2+} and Eu^{3+} ions, but with a substantial level of vacancy. Therefore, the Eu^{3+}-doped AWO_4 (A = Ca, Sr) compounds were confirmed with the formula of $A_{1-1.5x}Eu_x\square_{0.5x}WO_4$.

For **CELW** and **SELW** samples, the occupancy factors for Eu^{3+} and Li^+ were fixed as 0.24 and y, respectively. The final convergence of Rietveld refinements led to the occupancy factor of Ca^{2+}/Sr^{2+} to be 0.64-0.5y, considering a reasonable error of structure refinements. The final refinement results including atomic coordinates and isotropic thermal displacement factors are summarized in Table S1 in ESI. The final Rietveld refinement patterns of the selected samples of **CEW**, **SEW, CELW** and **SELW** are given in Fig. S4, together with the agreement factors. According to the Rietveld refinements, we confirmed the type I mechanism of the aliovalent doping in Ca^{2+}/Sr^{2+}-Scheelites. Therefore, in **SEW** and **CEW** solid solutions, the substitution of A^{2+} by Eu^{3+} created A-site vacancies according to the equation $3A^{2+} = 2A_{Eu}^{\cdot} + V_A''$.

Fig. 4 presents the detailed bond distances from the Rietveld refinements on selected samples. As mentioned above that the $Ca_{1-1.5x}Eu_x\square_{0.5x}WO_4$ ($0.04 \le x \le 0.24$) shows an interesting unit cell expansion when replacing Ca^{2+} by smaller Eu^{3+} cations (Ca^{2+}, 1.12 Å; Eu^{3+}, 1.066 Å), not to mention the increase of A-site vacancies. The structure refinements suggest that the Ca^{2+}/Eu^{3+}-oxygen average bond distance keeps almost unchanged when increasing x, while the W^{6+}-O bond distance tends to increase (from 1.837 (x = 0.04) Å to 1.870 (x = 0.24) Å). It is known that the former is a typical ionic bond and the latter is a covalent bond. When replacing a bivalent Ca^{2+} cation by a trivalent Eu^{3+} cation, the Eu^{3+} cation attracts oxygen ions apart from W^{6+}, resulting in the increase of W^{6+}-O bond distance. We believe this is the main factor to the expansion of unit cell volumes in $Ca_{1-1.5x}Eu_x\square_{0.5x}WO_4$ ($0.04 \le x \le 0.24$). Such an increase of W^{6+}-O bond distance was also observed in **SEW** and **SELW**, while the size difference between Sr^{2+} and Eu^{3+} is so significant that the average Sr/Eu-O bond distance shows a

clearly decreasing tendency and in the meantime, the unit cell shrinkage are also clearly observed.

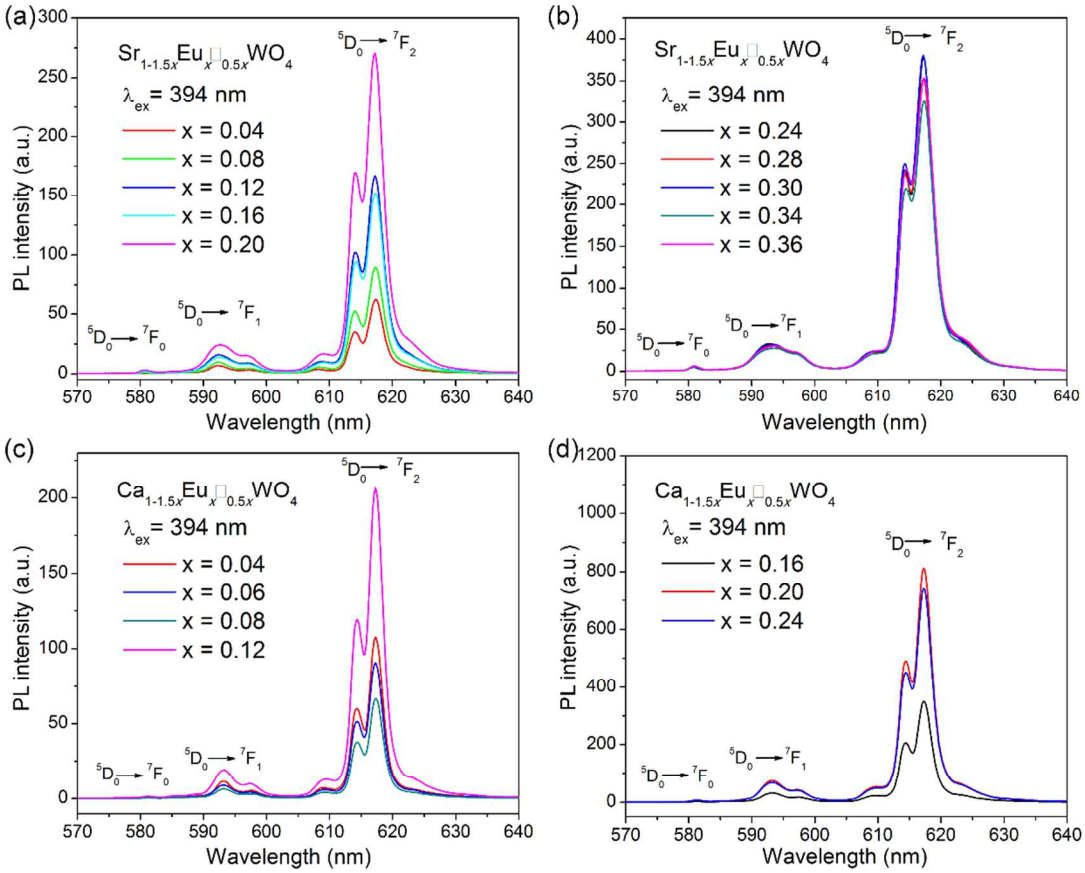

Fig. 6 Emission spectra excited by Eu^{3+} f-f transition (at 394 nm) for Eu^{3+}-doped AWO_4 (A = Ca, Sr) compounds.

In $Ca_{0.64-0.5y}Eu_{0.24}Li_y\square_{0.12-0.5y}WO_4$ ($0 \leq y \leq 0.24$), the incorporation of Li^+ leads to a moderate shrinkage of the unit cell volume (-1.6 Vol.%), comparing to the minor change in **CEW** (+0.6 Vol.%). The *A*-O and W-O bond distances almost kept constant. We speculate the real changes in bond distance are probably not significant enough and close to the accuracy of powder XRD refinements.

Luminescent properties of $A_{1-1.5x}Eu_x\square_{0.5x}WO_4$ (A = Ca or Sr)

The excitation spectra of **SEW** and **CEW** were measured from 200 to 550 nm by monitoring the strongest Eu^{3+} emission at 617 nm, as shown in Fig. 5. All of the excitation spectra show similar profiles, which consist an intense broad band (200-320 nm) and groups of narrow lines (350-550 nm). Obviously, the broad band consists two peaks (~240 and 275 nm), which means there are two interweaved excitation bands. According to references, the broad band is attributed to the combination of charge-transfer (CT) of $O^{2-} \rightarrow W^{6+}$ within the WO_4^{2-} group and $O^{2-} \rightarrow Eu^{3+}$. It is well known that, the CT excitation of Eu^{3+} is an electronic transition from the ground state to the excited state of 4*f* shell, and the corresponding band position is mainly determined by the co-valency of Eu-O bonds. Usually, an increasing in the bond co-valency would induce a blue-shifting of CT band. For Scheelites, the wavelength of $O^{2-} - Eu^{3+}$ CT state is calculated to be about 240 nm.[25] Therefore, the band with maximum at ~240 nm is assigned to the CT of $O^{2-} \rightarrow Eu^{3+}$; and the other band at higher wavelength (λ_{max} ~ 275 nm) is attributed to the CT of $O^{2-} \rightarrow W^{6+}$, respectively. The presence of CT band of $O^{2-} \rightarrow W^{6+}$ in the excitation spectra by monitoring Eu^{3+} emission, clearly suggests an energy transfer from WO_4^{2-} to Eu^{3+}. In addition, the narrow peaks in the wavelength range of 350-550 nm are characteristics of the *f-f* transitions of Eu^{3+}.

As shown in Fig. 5, although all of the absorption bands and peaks show the increasing tendency along with the increase of Eu^{3+} content, the growth of Eu^{3+} *f-f* transitions is much faster than that of CT bands. For instance, the intensities of the Eu^{3+} *f-f* excitation peaks are even higher than that of the CT band of $O^{2-} \rightarrow Eu^{3+}$ when *x* beyond 0.20 in **CEW**. It is also the major reason why Scheelites-based luminescent materials can be applied in UV-LED. Such intense *f-f* absorption implies the local environment of Eu^{3+} is far away from centrosymmetric. Additionally, the CT band of $O^{2-} \rightarrow W^{6+}$ shows a comparable enhancement with $O^{2-} \rightarrow Eu^{3+}$ CT band in both of SEW and CEW along with the increasing Eu^{3+} content, which means the energy transfer from WO_4^{2-} groups to Eu^{3+} ions becomes more efficient.

The composition-dependent photoluminescence (PL) emission spectra of **SEW** and **CEW** were given in Fig. 6, respectively, which were recorded from 570 to 640 nm under the excitation of 394 nm (*f-f* transition of Eu^{3+}). Three groups of emission peaks at 581, 587-600, and 605-630 nm were observed, which are attributed to the $^5D_0 \rightarrow {}^7F_J$ (J = 0, 1, 2) transitions of Eu^{3+} ion, respectively. In detail, the $^5D_0 \rightarrow {}^7F_0$ (at 581 nm) is a single peak, because there is only one crystallographic site for Eu^{3+} in the structure (*A*-site). The intensities of the peaks corresponding to $^5D_0 \rightarrow {}^7F_1$ transitions are much weaker than those of $^5D_0 \rightarrow {}^7F_2$ transitions, which is benefit for improving color purity of red phosphors. As is known, $^5D_0 \rightarrow {}^7F_1$ is a parity allowed magnetic dipole-dipole transition, and $^5D_0 \rightarrow {}^7F_2$ is a hypersensitive electric dipole-dipole transition. So, $^5D_0 \rightarrow {}^7F_2$ is very sensitive to the local environment, while $^5D_0 \rightarrow {}^7F_1$ is not. Therefore, the intensity ratio of $R/O = I(^5D_0 \rightarrow {}^7F_2)/I(^5D_0 \rightarrow {}^7F_1)$ is a structural probe of site symmetry for Eu^{3+}. Generally, a lower symmetry of the crystal field around Eu^{3+} leads to a larger R/O. For SEW and CEW, the R/O values are around 9.3 and 9.6 (see Fig. 7), respectively, which is a strong evidence that Eu^{3+} ions mainly occupy the lattice site without inversion symmetry.

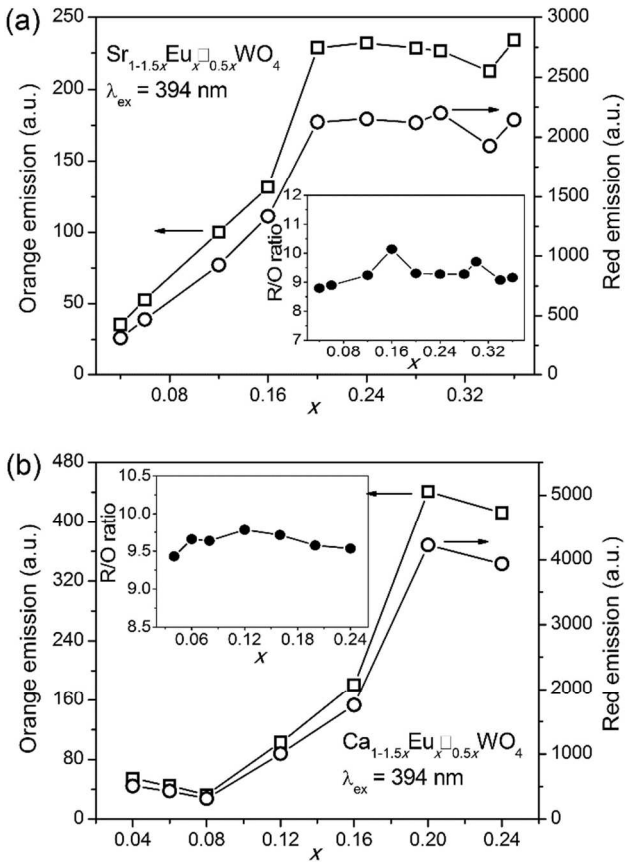

Fig. 7 The variation of the intensities of $^5D_0 \rightarrow {}^7F_1$ and $^5D_0 \rightarrow {}^7F_2$ transitions along with Eu^{3+} concentration for **SEW** and **CEW** when excited by 394 nm.

It is well known that both of $CaWO_4$ and $SrWO_4$ crystallize in the tetragonal Scheelite structure with the space group of $I4_1/a$, in which the *A* cation is coordinated by eight oxygen atoms with the S_4 point symmetry (no inversion center). In fact, it is reported in literature that the aliovalent Eu^{3+}-to-A^{2+} doping (together with the presence of the *A*-site vacancies in our case) could induce a local deviation of the site symmetry of Eu^{3+} from S_4 symmetry.[25] This is proved by the presence of very weak $^5D_0 \rightarrow {}^7F_0$ emission at 581 nm since this emission is only allowed for C_s, C_n, C_{nv} site symmetry.[37] Of course, the deviation of the S_4 symmetry of Eu^{3+} was also confirmed by the large R/O values.

For **SEW**, the emission intensities increases with Eu^{3+} content first, and then a saturation was observed in the range of x = 0.20 to 0.36 (Fig. 7a). As is known, non-radiative transition can occur in various routes, like between excited and unexcited Eu^{3+} ions, or from excited Eu^{3+}/WO_4 to defects. As discussed above, the content of *A*-site vacancies increases along with Eu^{3+} content, which means the vacancies are the main energy consumer in **SEW**. Therefore, the saturation of luminescence intensity for **SEW** indicates that the quenching effect is relatively weaker than the increase in the excited centers when Eu^{3+} concentration is low, and becomes comparable when x = 0.20. Similar emission saturation was also observed for **CEW**, as shown in Fig. 7b. However, the variation tendency of the emission intensity with x for **CEW** before saturation is slight different with that of **SEW**. A monotonic increase was observed for **SEW**, but for **CEW**, the luminescence intensity decreases slightly with increasing Eu^{3+} ion content firstly, and reach minimum when x = 0.08, and then increase with x till x = 0.20. Such a difference between **CEW** and **SEW** might be related with the different variety of the lattice parameters with x for these two series of compounds. First, the cell volume of **CEW** is much smaller than that of **SEW**; second, a significant shrinkage tendency was found for **SEW** with the increasing Eu^{3+} doping level, while the cell volume of **CEW** expands slightly along with x. In other words, the distance between *A*-cations is the shortest in un-doped $CaWO_4$ and becomes longer along with the increase of x. The relative short distance between *A*-cations in low Eu^{3+} concentrated **CEW** might increase the chance of cross-relaxation or energy transfer between excited and unexcited Eu^{3+} ions, which generates a slight concentration quenching.

Recently, a structure and luminescence study on $CaGd_{2(1-x)}Eu_{2x}(BO_4)_4$ (B = Mo, W) shows a similar phenomenon of luminescence saturation at x = 0.5, which means 25% of *A*-sites are occupied by Eu^{3+}.[38] The high concentration of activators for emission saturation is due to a relatively large Eu-Eu distances in Scheelite structure. Here in our cases of **CEW** and **SEW**, the increase of the Eu^{3+} also results in an increase of *A*-site vacancies, therefore the saturation occurs at a lower level of Eu^{3+} content (x = 0.2).

When excited by 274 nm (CT band of $O^{2-} \rightarrow W^{6+}$), the emission spectra show similar profiles but with lower intensities (Fig. S5, ESI). Fig. S6 shows the dependence of the emission intensities and R/O values of **SEW** and **CEW** under 274 nm excitation, which are also similar with those excited by 394 nm.

Luminescent properties of $A_{0.64-0.5y}Eu_{0.24}Li_y\square_{0.12-0.5y}WO_4$ (A = Ca or Sr)

$Ca_{0.64-0.5y}Eu_{0.24}Li_y\square_{0.12-0.5y}WO_4$ (**CELW**) and $Sr_{0.64-0.5y}Eu_{0.24}Li_y\square_{0.12-0.5y}WO_4$ (**SELW**) ($0 \le y \le 0.24$) were selected as represents for discussing the influence of the contents of Li^+ ion and A-site vacancy on the luminescence of Scheelites, where the Eu^{3+} content was kept as 0.24.

The excitation spectra of ***A*ELW** phosphors were given in Fig. S7, which show similar profiles with that of **CEW** and **SEW**. The intense *f-f* absorptions of Eu^{3+} confirms the non-centrosymmetric local environment of Eu^{3+}. The emission spectra of ***A*ELW** phosphors under 394 nm excitation were shown in Figs. 8a and 8b, which also show similar profile with that of SEW and CEW. Figs. 8c and 8d give the dependences of the emission intensities and *R*/*O* values of **SELW** and **CELW** along with the Li^+ content, where a similar changing tendency was observed. Taking **SELW** as a representative, the emission intensity increases with the increasing of the Li^+ concentration and reaches the maximum when y = 0.20, and then decrease slightly when y = 0.24. Comparing to **SEW**, the enhancement for luminescence by co-doping Li^+ as charge compensating ion

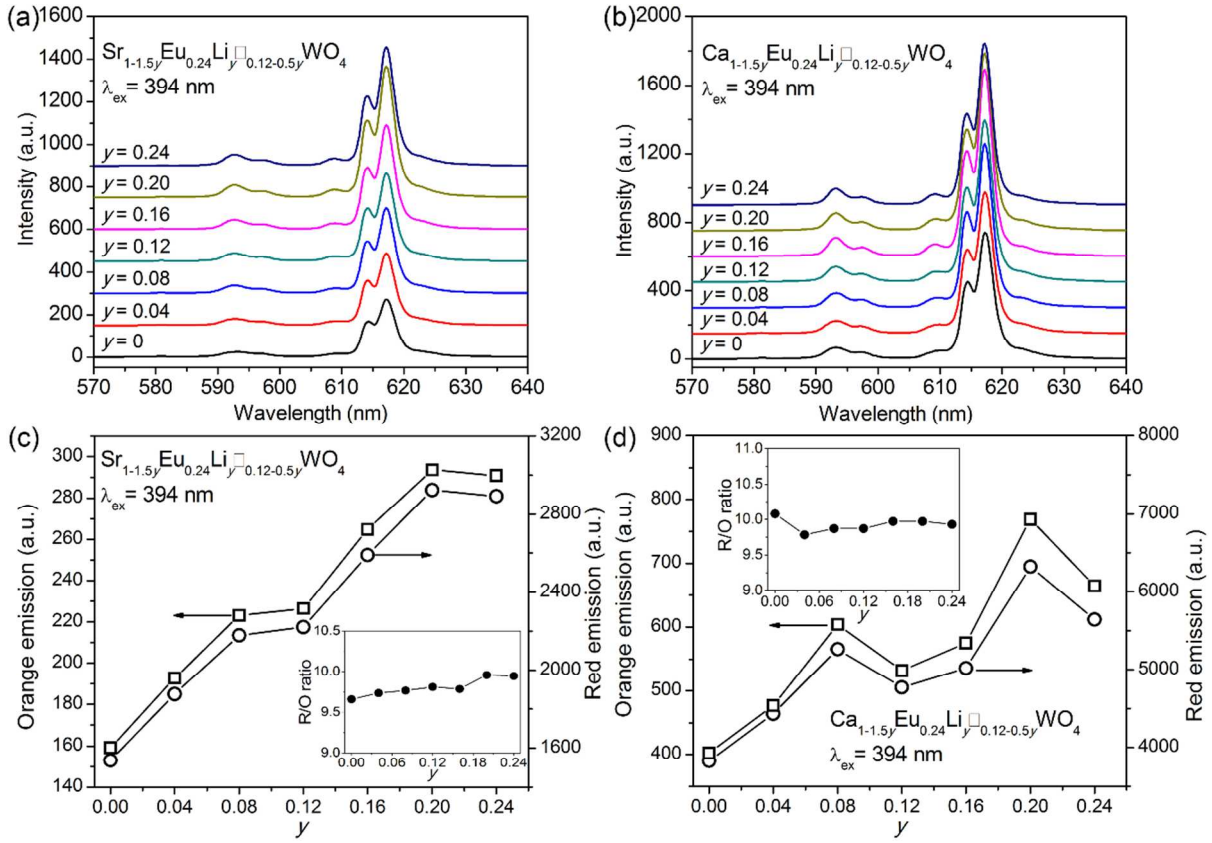

Fig. 8 (a, b) The Emission spectra for Eu^{3+}/Li^+ co-doped $SrWO_4$ and $CaWO_4$ samples, where the spectra were shift along the y-axis for better presentation; (c, d) the intensities for red and orange emission along with the content of Li^+, and the R/O ratios are also shown in the inserts.

has been reported for many times, and it was due to the modification of the coordination environment of Eu^{3+} by Li^+-incorporation. In $Sr_{0.64-0.5y}Eu_{0.24}Li_y\square_{0.12-0.5y}WO_4$ ($0 \le y \le 0.24$), the concentration of A-site vacancy is related with the content of Li^+. When y = 0, the content of vacancy has the maximum value of 0.12; if y = 0.24, there is no vacancy. In other words, the content of vacancy decreases along with the increase of Li^+ concentration. It is known that vacancies are the trapping centers of the excited energy, therefore, it becomes understandable that the emission was enhanced when increasing the content of Li^+ in **SELW**. For example, the emission intensity of the sample with y = 0.20 is 2.5 times of that of $Sr_{0.64}Eu_{0.24}WO_4$ (see Fig. 8c).

The color purity of these phosphors was also studied. As shown in the inserts in Figs. 8c and 8d, the *R*/*O* ratios for **SELW** and **CELW** are both ~10, which are slightly larger than that of **SEW and CEW**. Such a variety implies the local coordination environment around Eu^{3+} is modified by Li^+ ions. In summary, the emission intensity and color purity of **SELW** and **CELW** phosphors are both improved due to the incorporation of Li^+, which makes these compounds suitable as red phosphors for UV-LED application.

Conclusion

$A_{1-1.5x}Eu_x\square_{0.5x}WO_4$ and $A_{0.64-0.5y}Eu_{0.24}Li_y\square_{0.12-0.5y}WO_4$ (A = Ca, Sr; □ = vacancy) were prepared by high temperature solid state reaction. All solid solutions show a linear change of the cell volume confirming the successful doping. It is important to pin down the charge balance mechanism, where A-site

vacancies were proved by Rietveld refinements. In addition, all samples crystallize in $I4_1/a$ with a disordering arrangement of A^{2+}, Eu^{3+}, □ at A-site. An abnormal unit cell expansion in $Ca_{1-1.5x}Eu_x□_{0.5x}WO_4$ was observed, where the expansion of WO_4 tetrahedra was caused by the replacement of the bivalent Ca^{2+} by trivalent Eu^{3+}. The title compounds are all good red phosphors with high R/O ratio, indicating that Eu^{3+} locates at a significantly distorted cavity. Both **SEW** and **CEW** show a saturation phenomenon at a high doping level, x = 0.20. With the incorporation of Li^+, the emission intensity was generally enhanced comparing to the Li^+-free samples, moreover, the increasing of Li^+ content in **AELW** phosphors reduce the content of vacancy, resulting in an further increasing of the luminescent intensity.

Acknowledgements

This work was financially supported by the Nature Science Foundation of China (Grants 91222106, 21101175, 21171178) and Natural Science Foundation Project of Chongqing (Grants 2012jjA0438, 2014jcyjA50036). The Fundamental Research Funds for the Central Universities (Grant CQDXWL-2014-005) also partially supported this work.

Notes and references

[a] College of Chemistry and Chemical Engineering, Chongqing University, Chongqing 400044, People's Republic of China. Corresponding author, Email: congrihong@cqu.edu.cn, taoyang@cqu.edu.cn; Tel: +86-23-65105065.

Electronic Supplementary Information (ESI) available: XRD patterns for "$Sr_{0.92}Eu_{0.08}WO_{4.04}$" and "$Ca_{0.90}Eu_{0.10}WO_{4.05}$", AC impedance spectra for "$Ca_{0.7}Eu_{0.22}WO_{4.03}$", Rietveld refinement plots, and so-obtained structure parameters. See DOI: 10.1039/b000000x/

1. A. Jayaraman, G. A. Kourouklis, L. G. Vanuitert, W. H. Grodkiewicz, R. G. Maines, *Phys. A*, 1989, **156**, 325-340.
2 L. Birbenbach, F. Buschendorf, *Zeitschrift fuer physikalische chemie*, 1936, **16**, 102-112.
3 A. Jayaraman, S. W. Wang, S. K. Sharma, *Phys. Rev. B*, 1995, **52**, 9886-9889.
4 A. Jayaraman, S. Y. Wang, S. K. Sharma, *Curr. Sci.*, 1995, **69**, 44-48.
5 A. Jayaraman, B. Batlogg, L. G. V., *Phys. Rev. B*, 1985, **31**, 5423-5472.
6 X. Wang, I. Loa, K. Syassen, M. Hanfland, B. Ferrand, *Phys. Rev. B*, 2004, **70**, 064109.
7 U. K. Trunov, V. A. Efremov, *Kristallografiyar*, 1981, **26**, 67-71.
8 M. Hirano, H. Morikawa, *Chem. Mater.*, 2003, **15**, 2561-2566.
9 V. A. Morozov, A. V. Arakcheeva, G. Chapuis, N. Guiblin, M. D. Rossell, G. Van Tendeloo, *Chem. Mater.*, 2006, **18**, 4075-4082.
10 Y. F. Chen, M. L. Ku, L. Y. Tsai, and Y. C. Chen, *Opt. lett.*, 2004, **29**, 2279-2281.
11 A. S. Grabtachikov, A. N. Kuzmin, V. A. Lisinetskii, V. A. Orlovich, G. I. Ryabtsev, A. A. Demidovich, *Appl. Phys. Lett.*, 1999, **75**, 3742-3744.
12 R. J. Packer, S. J. Skinner, A. A. Yaremchenko, E. V. Tsipis, V. V. Kharton, M. V. Patrakeev, Y. A. Bakhteeva, *J. Mater. Chem.*, 2006, **16**, 3503-3511.
13 T. Esaka, T. Mina-ai, H. Iwahara, *Solid State Ionics*, 1992, **57**, 319-325.
14 S. Takai, K. Sugiura, T. Esaka, *Mater. Res. Bull.*, 1999, **34**, 193-202.
15 Y. Yong, B. C. Fa, W. T. Yan, S. L. Liao, *J. Lumin.*, 2011, **131**, 1140-1143.
16 Z. H. Ju, R.P. Wei, X. P. Gao, W. S. Liu, C. R. Pang, *Opt. Mater.*, 2011, **33**, 909-913.
17 F. Kang, Y. Hu, L. Chen, X. Wang, Z. Mu, H. Wu, G. Ju, *Appl. Phys. B*, 2012, **107**, 833-837.
18 C. C. Zhao, X. Yin, F. Q. Huang, Y. Hang, *J. Solid State Chem.*, 2011, **184**, 3190-3194.
19 M. Mai, C. Feldmann, *J. Mater. Sci.*, 2012, **47**, 1427-1435.
20 S. Neeraj, N. Kijima, A.K. Cheetham, *Chem. Phys. Lett.*, 2004, **387**, 2-6.
21 Y. B. Zeng, Z. Q. Li, L. M. Wang, Y. J. Xiong, *CrystEngComm.*, 2012, **14**, 7043-7048.
22 F. Lei, B. Yan, *J. Solid State Chem.*, 2008, **181**,855-862.
23 Y. Q. Chen, B. K. Moon, B. C. Choi, J. H. Jeong, H. K. Yang, *J. Am. Ceram. Soc.*, 2013, **96**, 3596-3602.
24 Q. Zhang, Q. Y. Meng, W. J. Sun, *Opt. Mater.*, 2013, **35**, 915-922.
25 Y. G. Su, L. P. Li, G. S. Li, *Chem. Mater.* 2008**, 20**, 6060-6067.
26 S. K. Shi, J. Gao, J. Zhou, *Opt. Mater.*, 2008, **30**, 1616-1620.
27 S. W. Cho, *Bull. Korean Chem. Soc.*, 2013, **34**, 2769-2773.
28 A. F. VandenElzen, G. D. Rieck, *Acta Crystallagr.*, 1973, **29**, 2433-2436.
29 M. Gartner, D. Abeln, A. Pring, M. Wilde, A. Reller, *J. Solid State Chem.*, 1994, **111**, 128-133.
30 W. Jeitschko, *Acta Cryst. B*, 1973, **29**, 2074-2081.
31 TOPAS, V4.1-beta, Bruker AXS, Karlsruhe, Germany, 2004.
32 D. H. Templeton, A. Zalkin, *Acta Crystallagr.*, 1963, **16**, 762-766.
33 V. A. Morozova, A. V. Mironov, B. I. Lazoryak, E. G. Khaikina, O. M. Basovich, M. D. Rossell, G. Van Tendeloo, *J. Solid State Chem.*, 2006, **179**, 1183-1191.
34 V. A. Morozov, A. Arakcheeva, B. Redkin, V. Sinitsyn, S. Khasanov, E. Kudrenko, M. Raskina, O. Lebedev, G. Van Tendeloo, *Inorg. Chem.*, 2012, **51**, 5313-5324.
35 A. M. Abakumov, V. A. Morozov, A. A. Tsirlin, J. Verbeeck, J. Hadermann, *Inorg. Chem.*, 2014, **53**, 9407-9415.
36 A. Arakcheeva, D. Logvinovich, G. Chapuis, V. Morozov, S. V. Eliseeva, J. C. G. Bunzli, P. Pattison, *Chem. Sci.*, 2011, **3**, 384-390.
37 G. Blass, A. Bril, *Philips Res. Rep.* 1966, **2**, 268.
38 V. A. Morozov, A. Bertha, K. W. Meert, S. Van Rompaey, D. Batuk, G. T. Martinez, S. Van Aert, P. F. Smet, M. V. Raskina, D. Poelman, A. M. Abakumov, J. Hadermann, *Chem. Mater.* 2013, **25**, 4387-4395.

Graphical Abstract for

Structural investigation of the *A*-site vacancy in Scheelites and the luminescence behaviors of two continuous solid solutions $A_{1-1.5x}Eu_x\square_{0.5x}WO_4$ and $A_{0.64-0.5y}Eu_{0.24}Li_y\square_{0.12-0.5y}WO_4$ (*A* = Ca, Sr; □ = vacancy)

Pengfei Jiang, Wenliang Gao, Rihong Cong,* and Tao Yang*

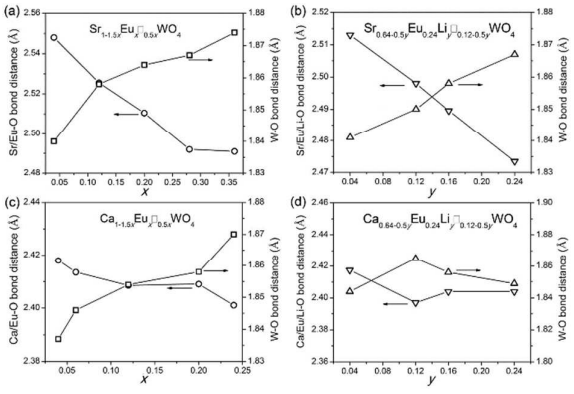

A detailed structural characterizations on $A_{1-1.5x}Eu_x\square_{0.5x}WO_4$ and $A_{0.64-0.5y}Eu_{0.24}Li_y\square_{0.12-0.5y}WO_4$ (*A* = Ca, Sr; □ = vacancy) prove the *A*-site vacancy mechanism for charge balance.

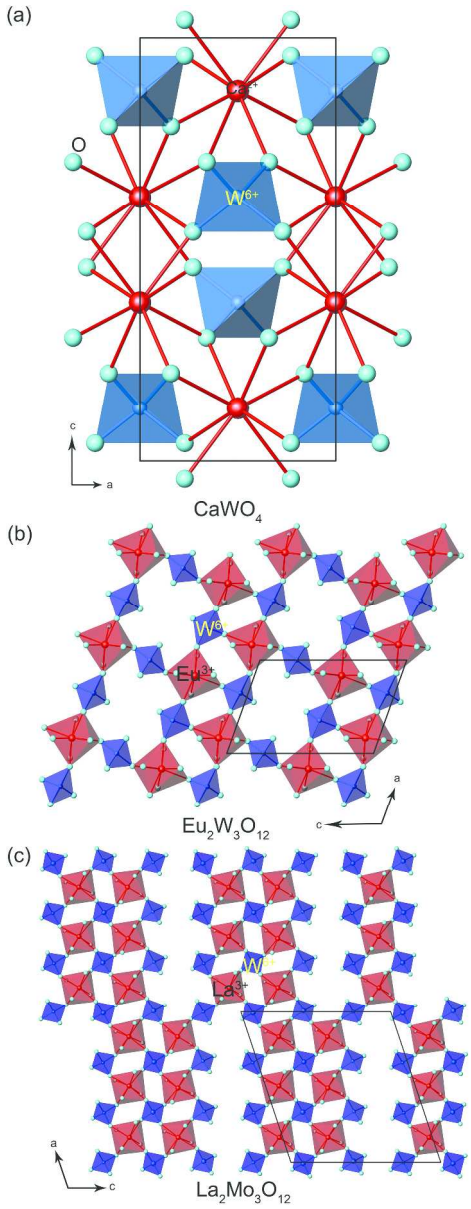

Fig. 1 (a) An example of tetragonal Scheelite structure; two representatives showing vacancy-ordered Scheelite structure (b) Eu2W3O12 and (c) La2Mo3O12.
296x769mm (300 x 300 DPI)

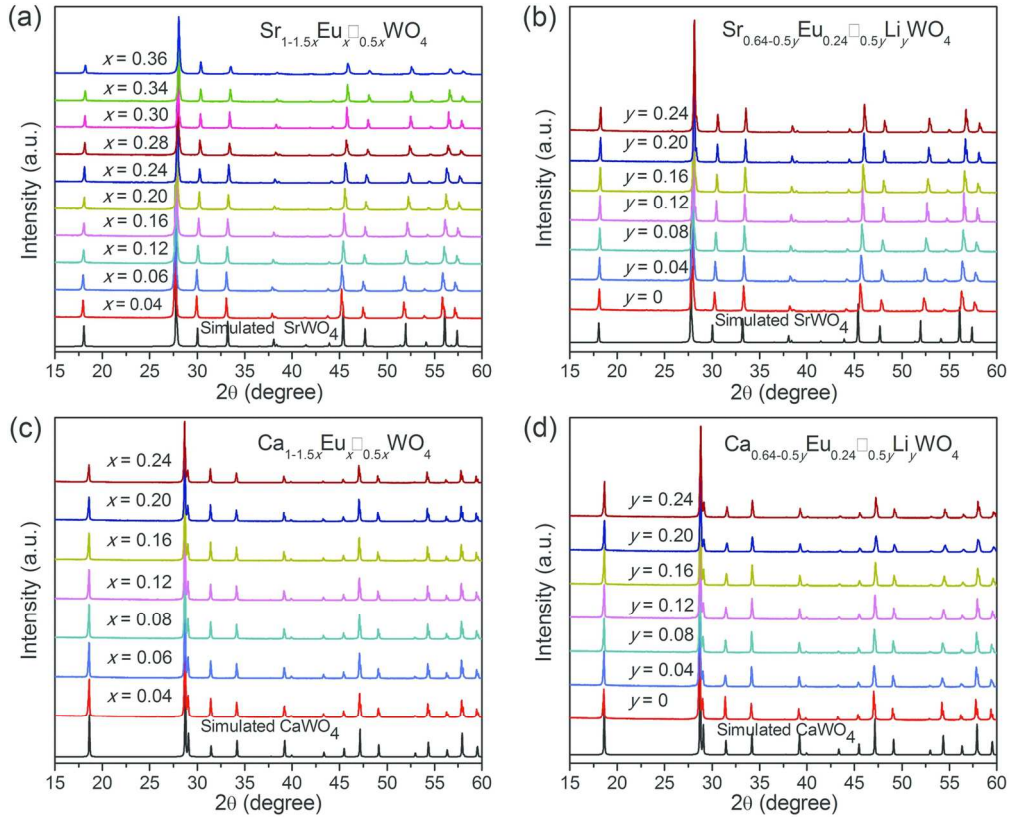

Fig. 2 XRD patterns for Eu3+-doped and Eu3+/Li+-co-doped Scheelite compounds. Simulated patterns for SrWO4 and CaWO4 based on structures are shown as reference.
144x117mm (300 x 300 DPI)

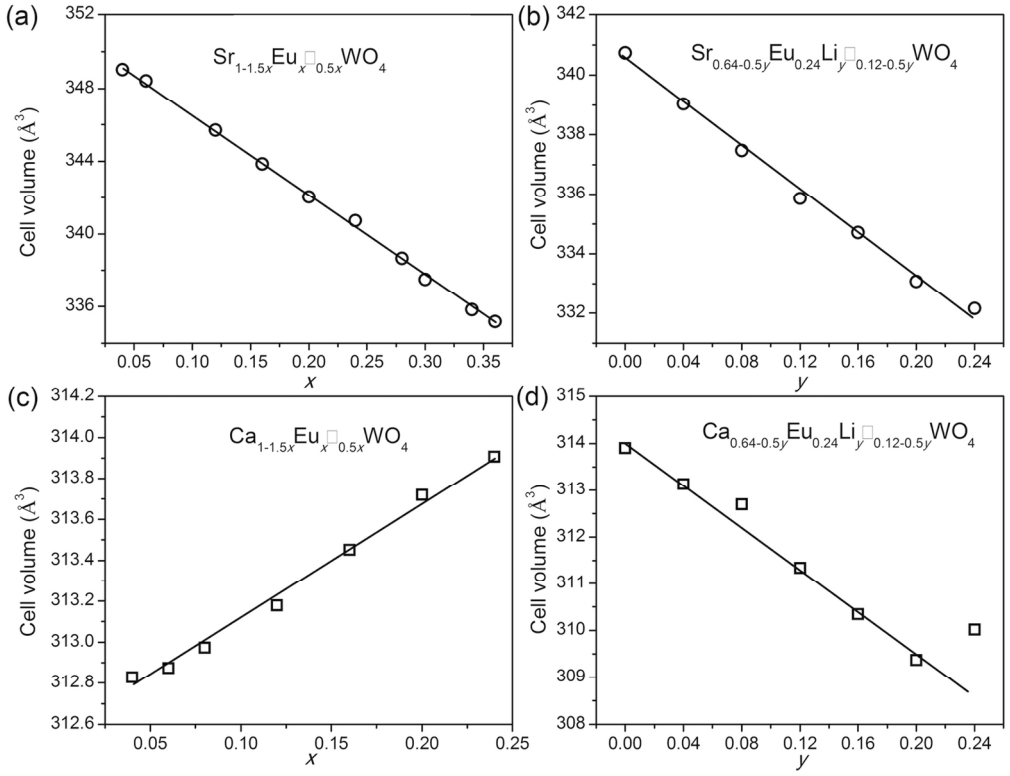

Fig. 3 Calculated cell volumes by Le Bail fitting on whole XRD patterns of title compounds.
136x104mm (300 x 300 DPI)

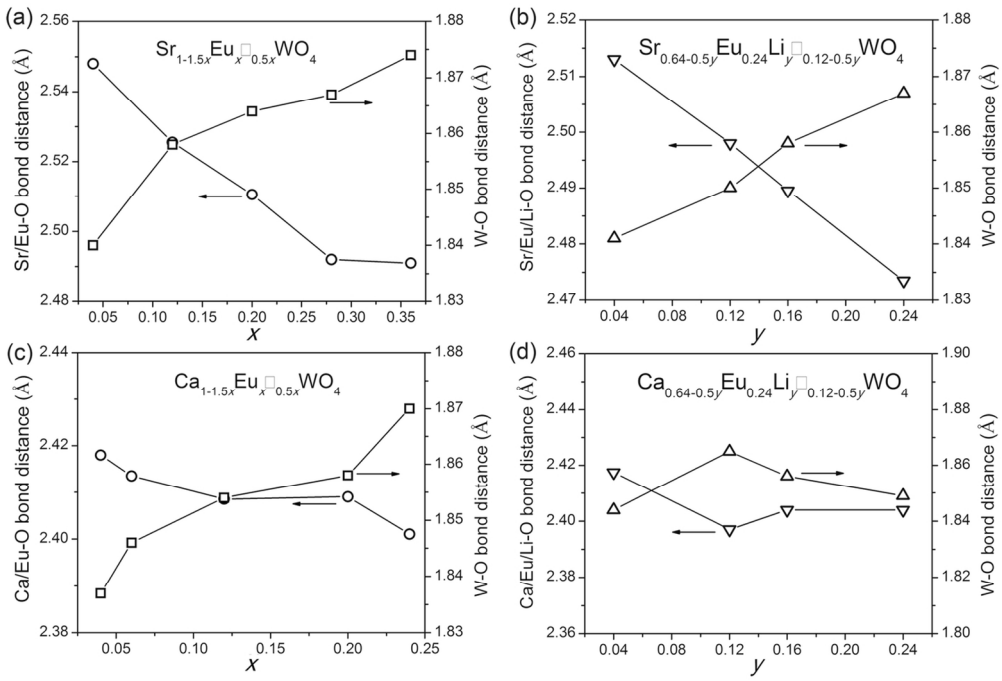

Fig. 4 Average bond distances of A-O and W-O for selected samples.
120x81mm (300 x 300 DPI)

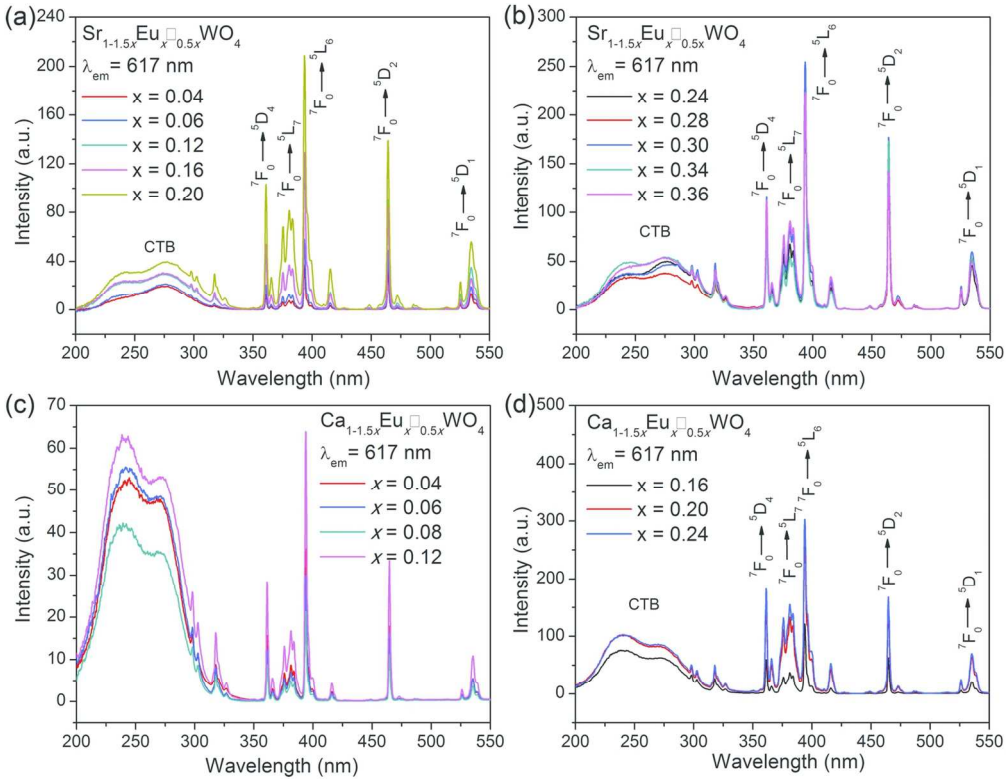

Fig. 5 Excitation spectra by monitoring the emission at 617 nm for Eu3+-doped SrWO4 and CaWO4 samples.
137x106mm (300 x 300 DPI)

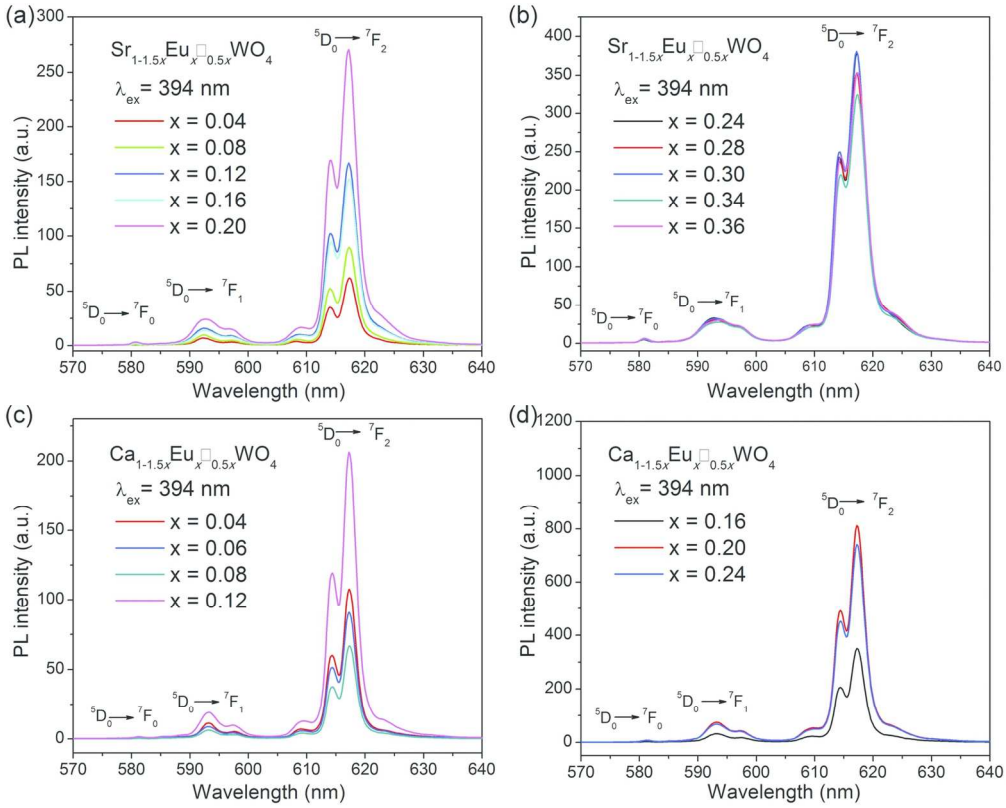

Fig. 6 Emission spectra excited by Eu3+ f-f transition (at 394 nm) for Eu3+-doped AWO4 (A = Ca, Sr)¬ compounds.
142x114mm (300 x 300 DPI)

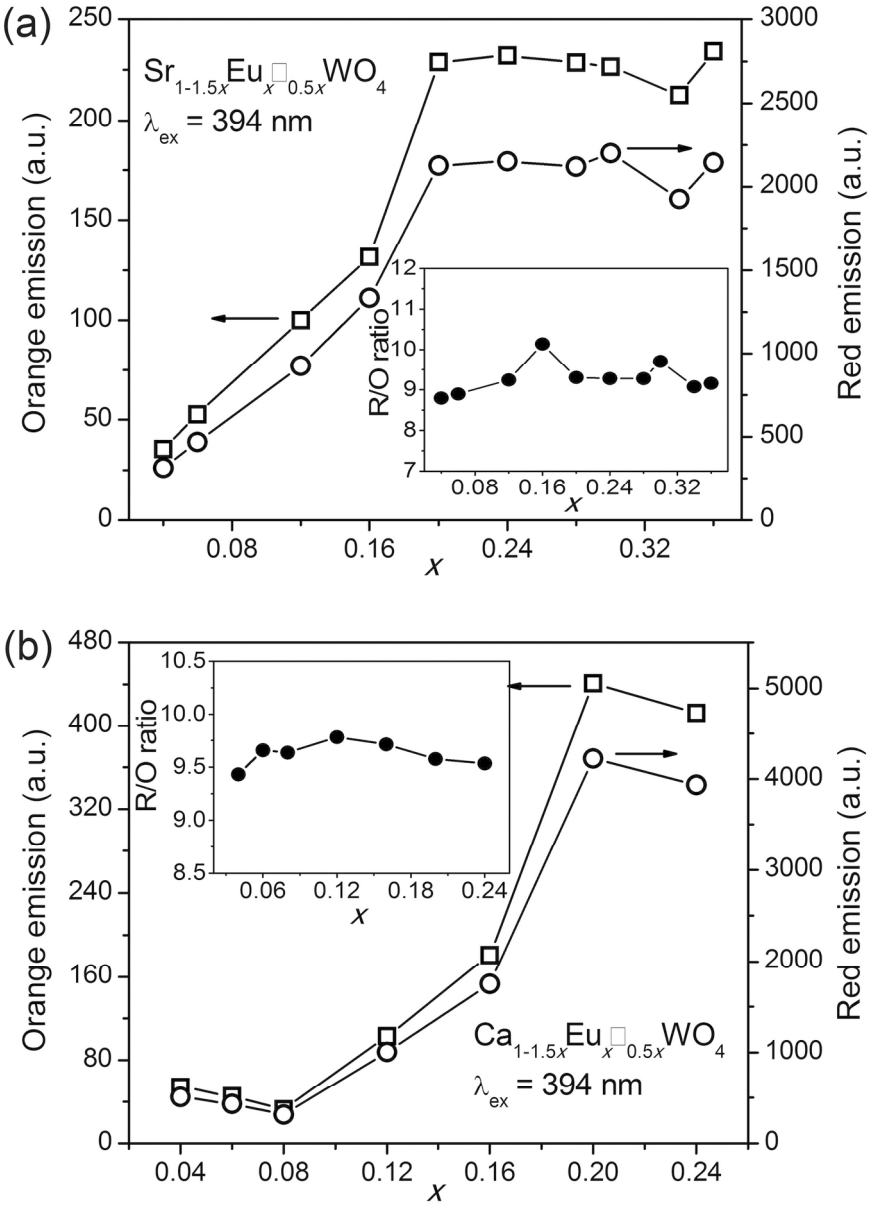

Fig. 7 The variation of the intensities of 5D0 → 7F1 and 5D0 → 7F2 transitions along with Eu3+ concentration for SEW and CEW when excited by 394 nm.
148x205mm (300 x 300 DPI)

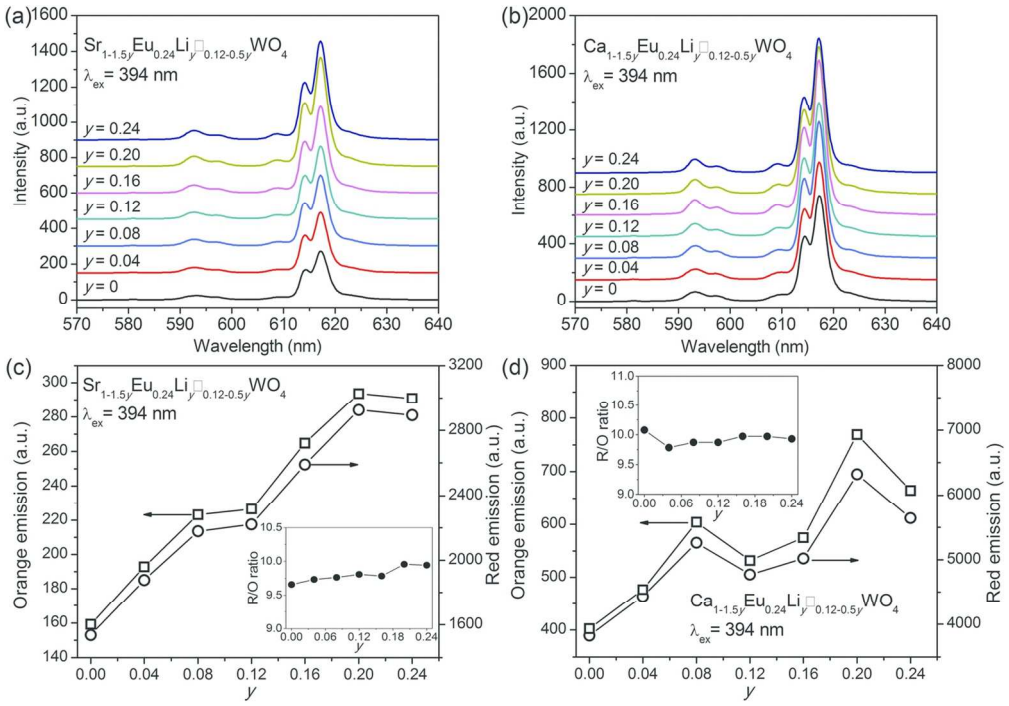

Fig. 8 (a, b) The Emission spectra for Eu3+/Li+ co-doped SrWO4 and CaWO4 samples, where the spectra were shift along the y-axis for better presentation; (c, d) the intensities for red and orange emission along with the content of Li+, and the R/O ratios are also shown in the inserts.
128x89mm (300 x 300 DPI)

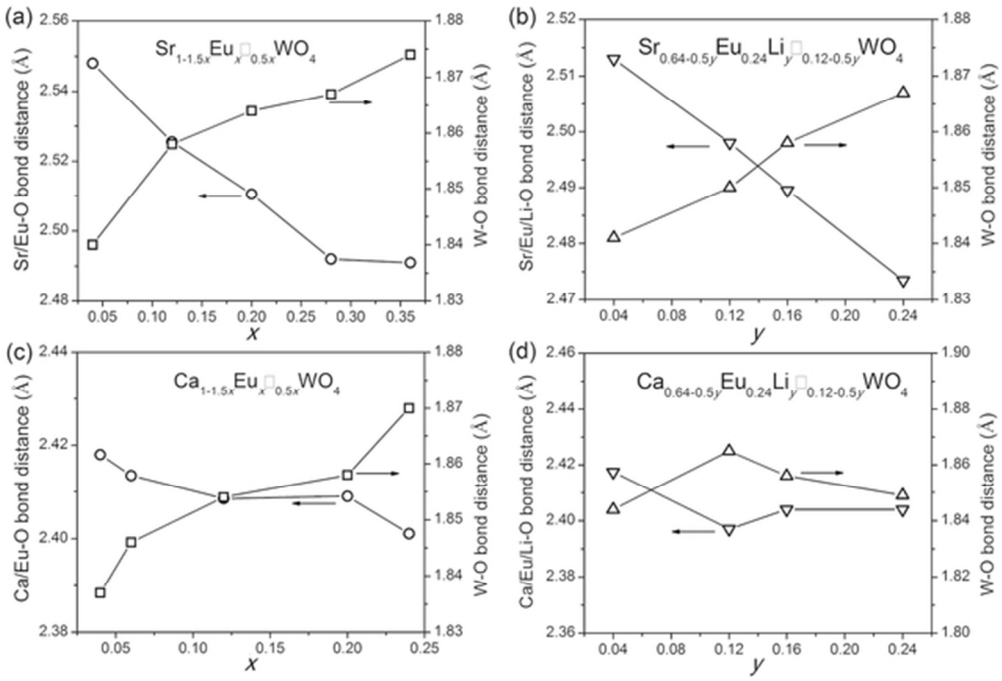

Graphic Abstract Figure
54x36mm (300 x 300 DPI)

Electronic Supplementary Information for

Structural investigation of the *A*-site vacancy in Scheelites and the luminescence behaviors of two continuous solid solutions $A_{1-1.5x}Eu_x\square_{0.5x}WO_4$ and $A_{0.64-0.5y}Eu_{0.24}Li_y\square_{0.12-0.5y}WO_4$ (A = Ca, Sr; □ = vacancy)

Pengfei Jiang, Wenliang Gao, Rihong Cong, and Tao Yang**

College of Chemistry and Chemical Engineering, Chongqing University, Chongqing 400044, P. R. China

*Correspondence authors, Email: congrihong@cqu.edu.cn and taoyang@cqu.edu.cn; Tel: (8623)65105065, Fax: (8623)65105065.

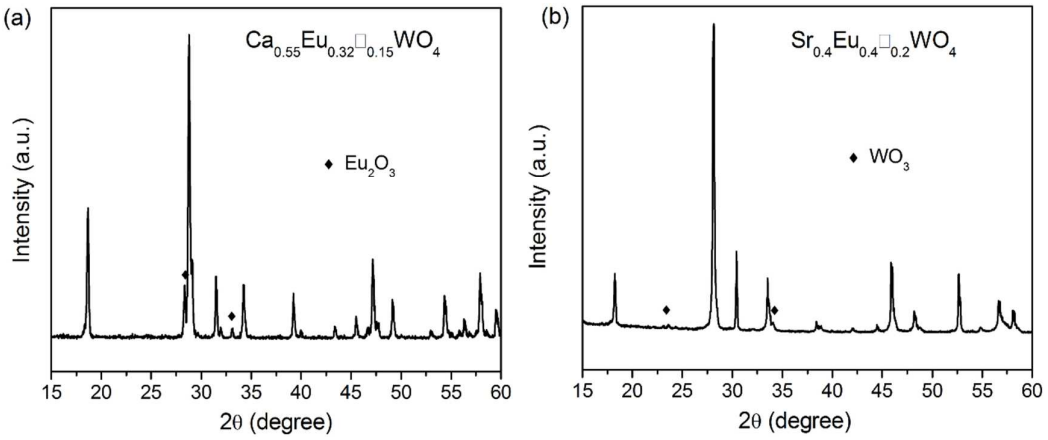

Fig. S1 XRD patterns for "$Ca_{0.55}Eu_{0.32}\square_{0.15}WO_4$" and "$Sr_{0.4}Eu_{0.4}\square_{0.2}WO_4$" samples prepared by high temperature solid state reactions. Other than the major phase of Scheelite, minor impurity peaks appear as marked in above figures, either belong to Eu_2O_3 or WO_3. There supposed to be other impurities, however, probably their diffraction peaks are overlapped with the major phase, it is hard to identify all of them. Nevertheless, our experiments show that the assumed compositions "$Ca_{0.55}Eu_{0.32}\square_{0.15}WO_4$" and "$Sr_{0.4}Eu_{0.4}\square_{0.2}WO_4$" cannot be annealed to be phase-pure.

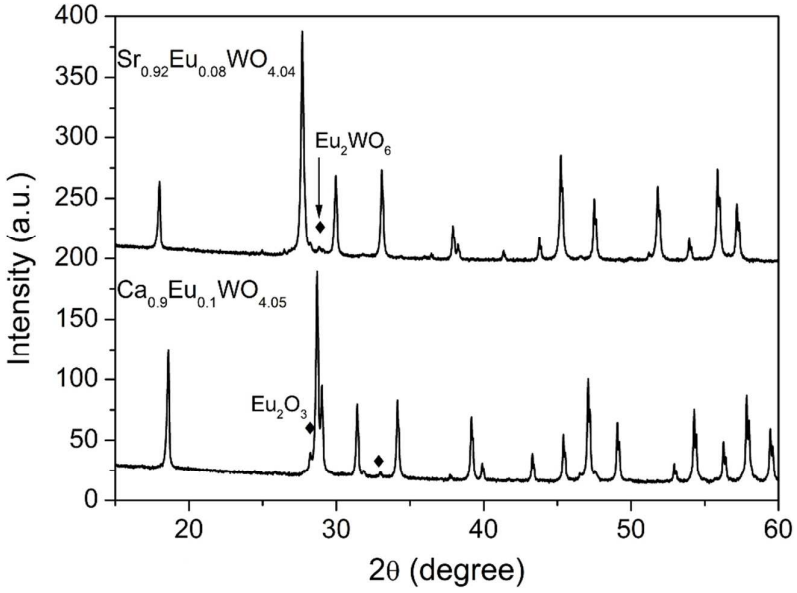

Fig. S2 XRD patterns of $Sr_{0.92}Eu_{0.08}WO_{4.04}$ and $Ca_{0.90}Eu_{0.10}WO_{4.05}$. The dark diamond in the figure represents the diffraction peaks of the impurity phases.

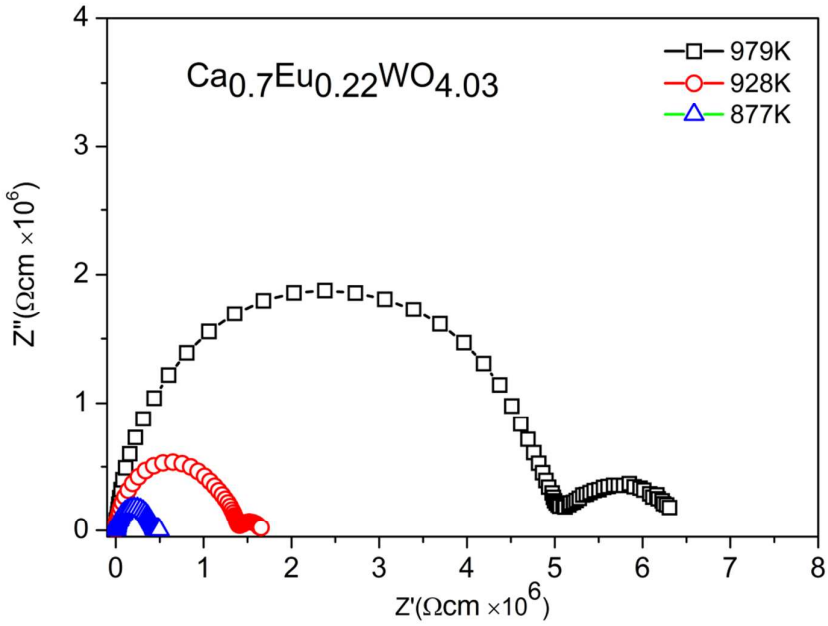

Fig. S3 Complex AC impedance spectra at 600, 650 and 705 ^{o}C, which comprise one broad and one narrow semi-circles. The broad and narrow semi-circle assign to the bulk and grain boundary contribution, respectively, and no electrode response or ionic conductivity was observed.

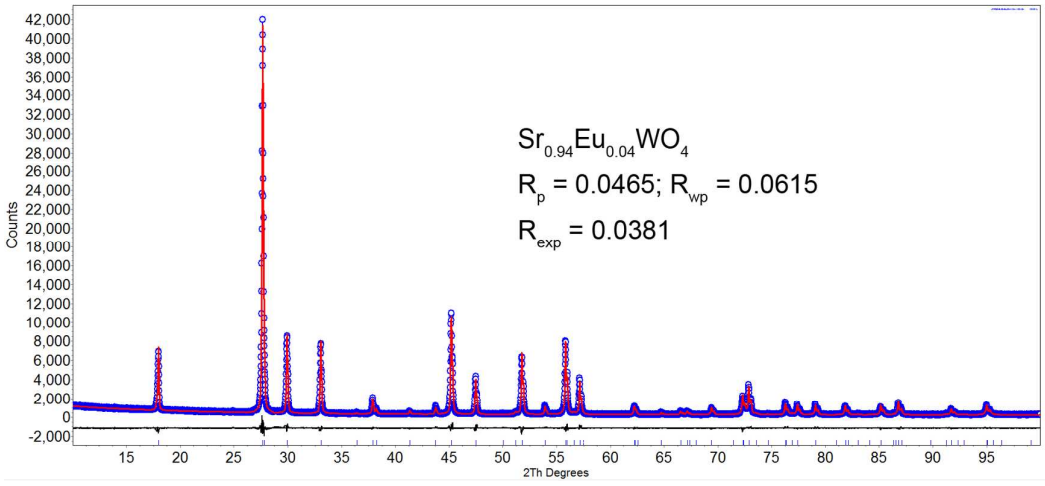

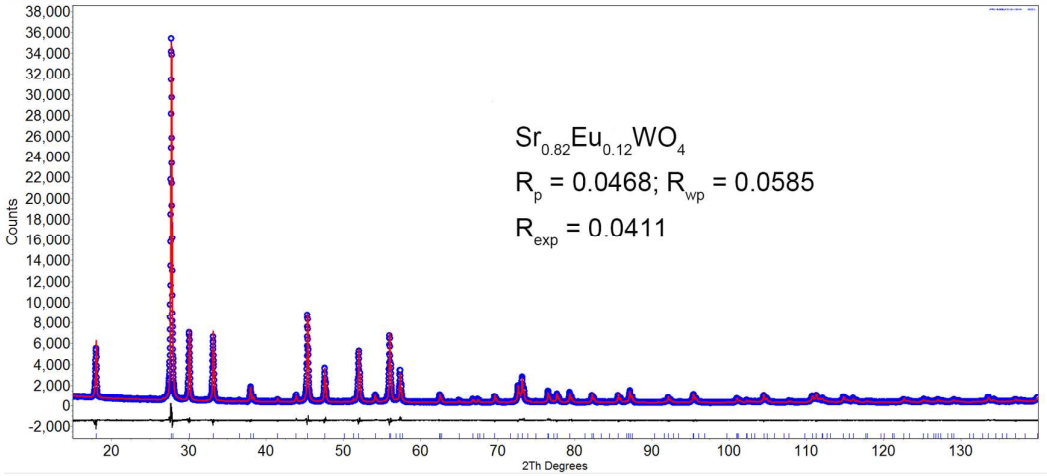

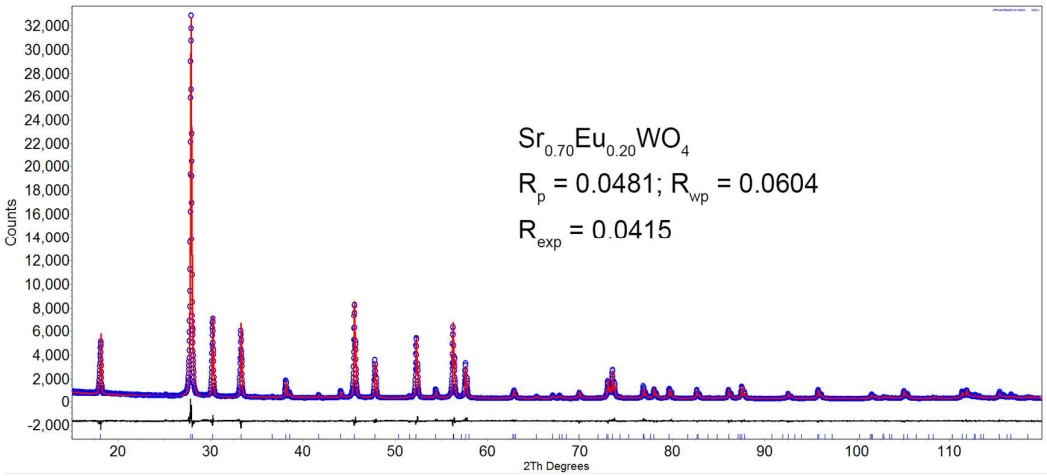

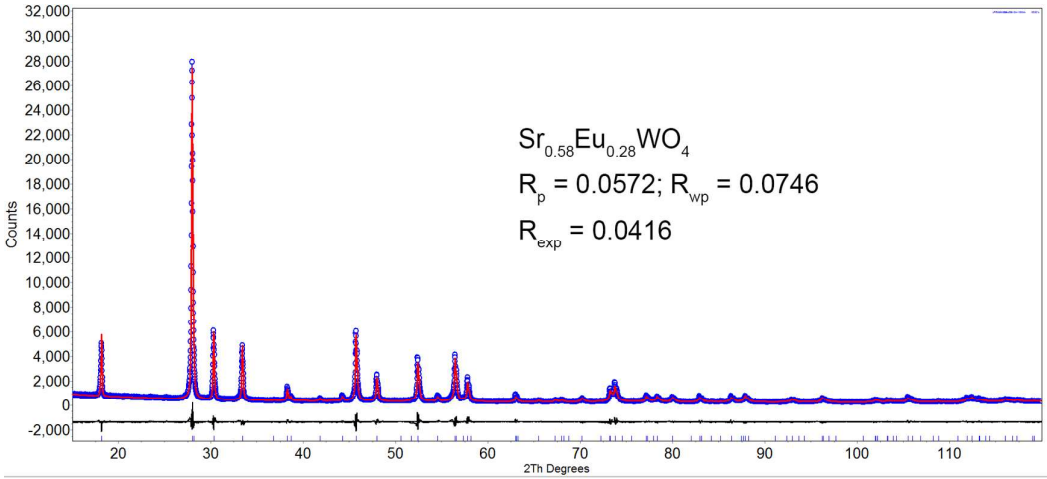

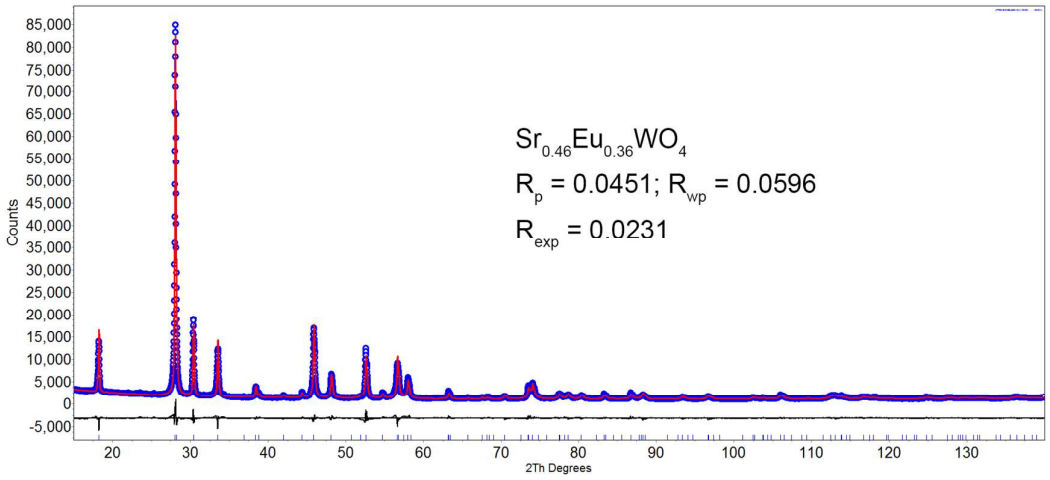

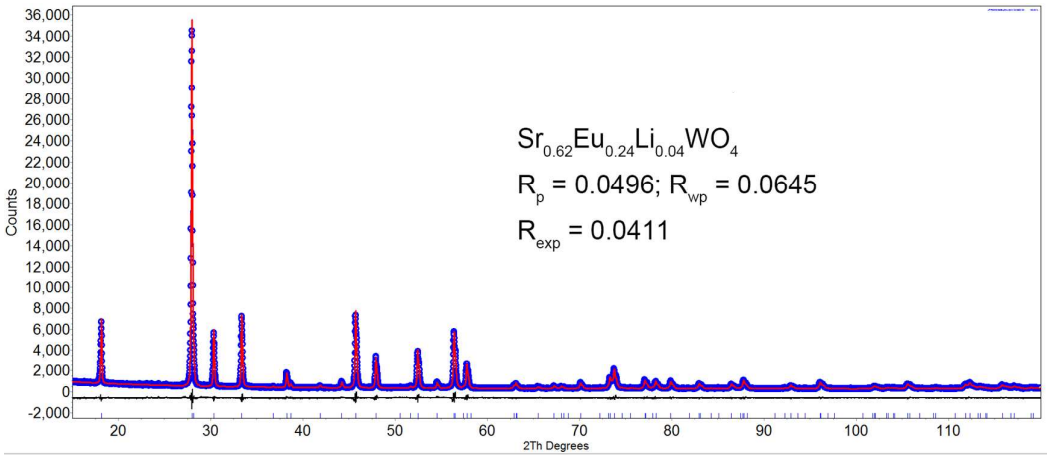

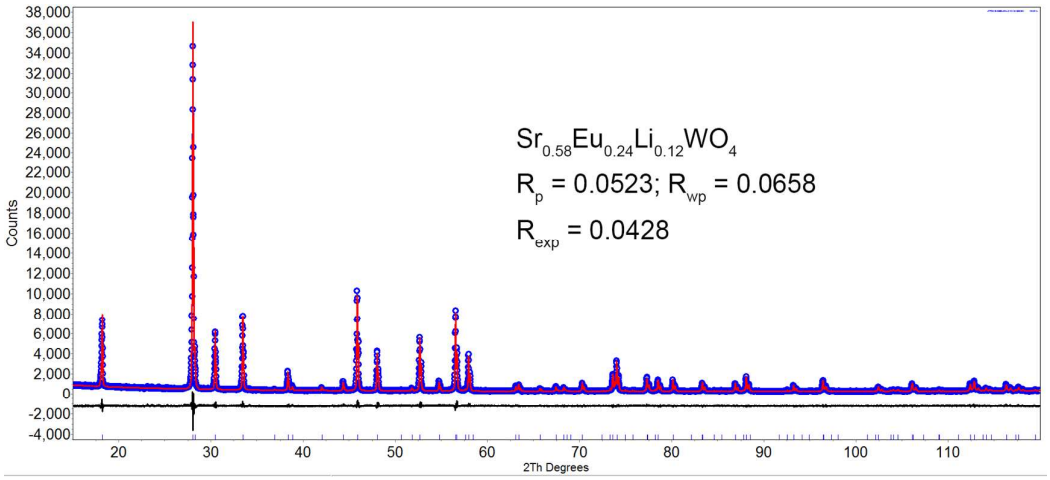

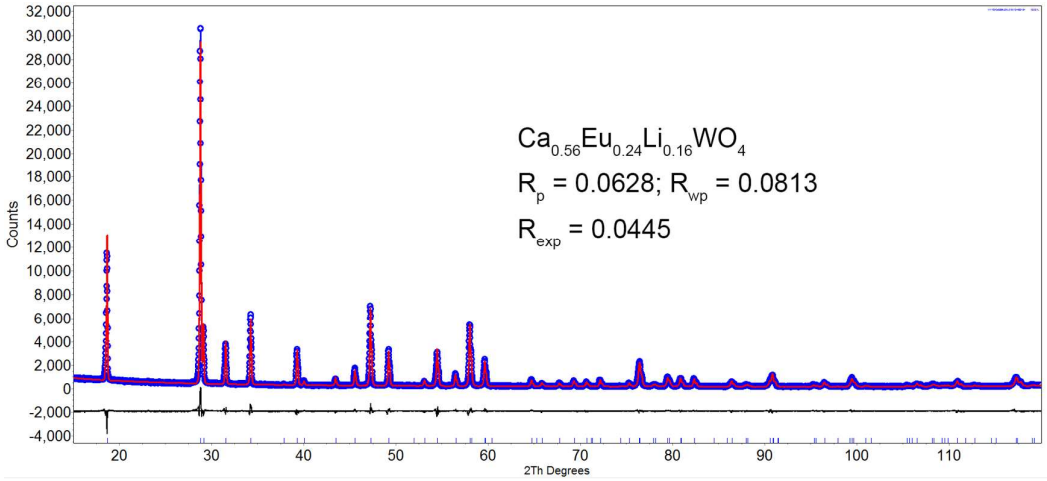

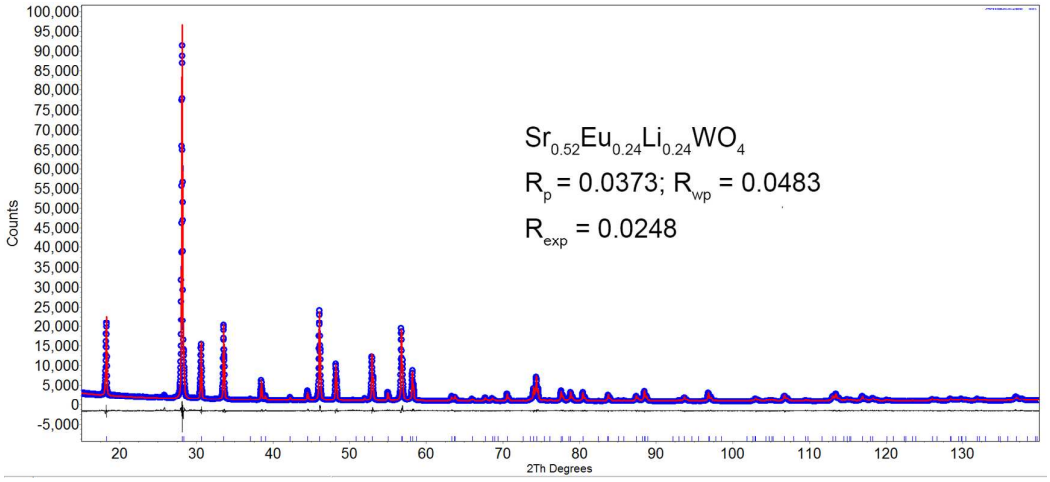

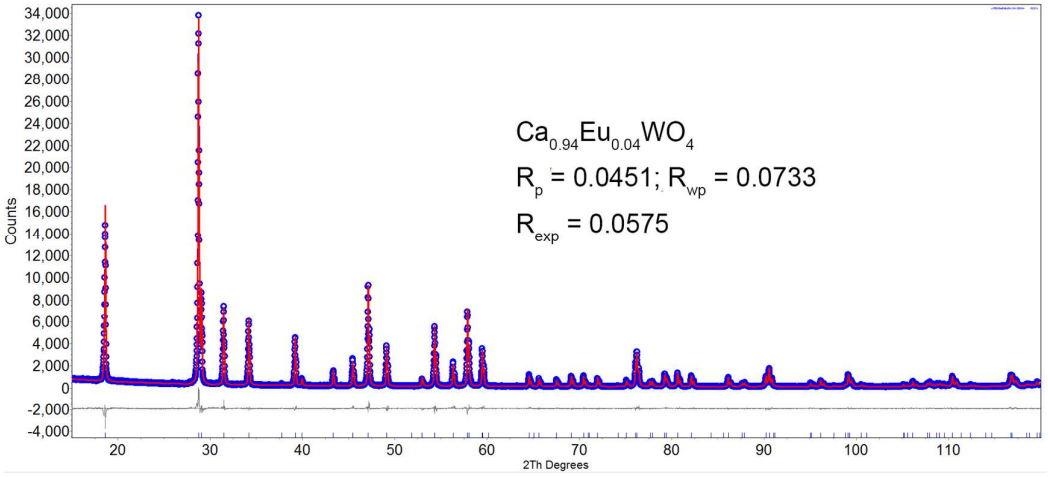

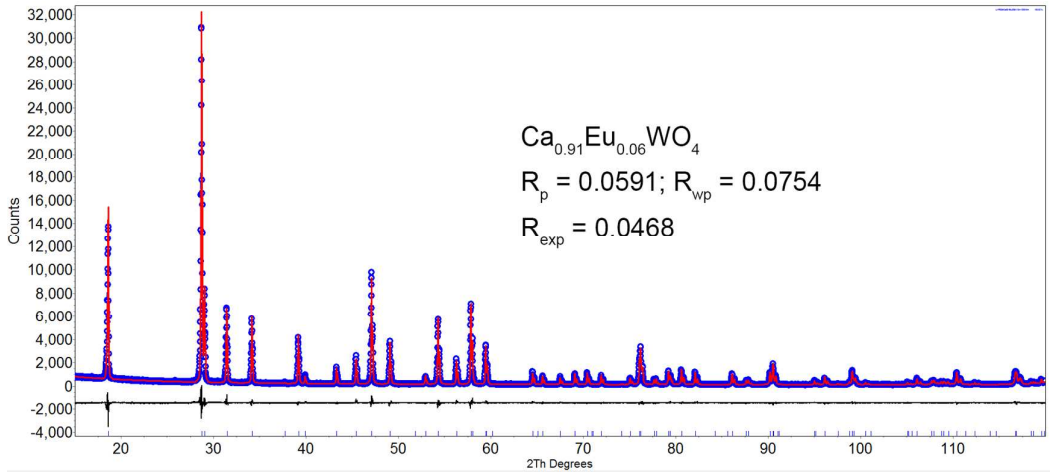

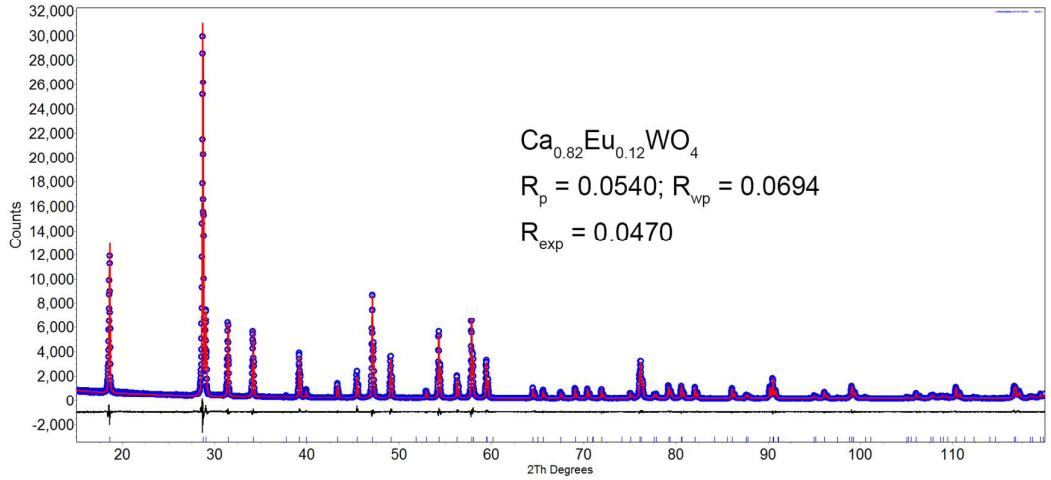

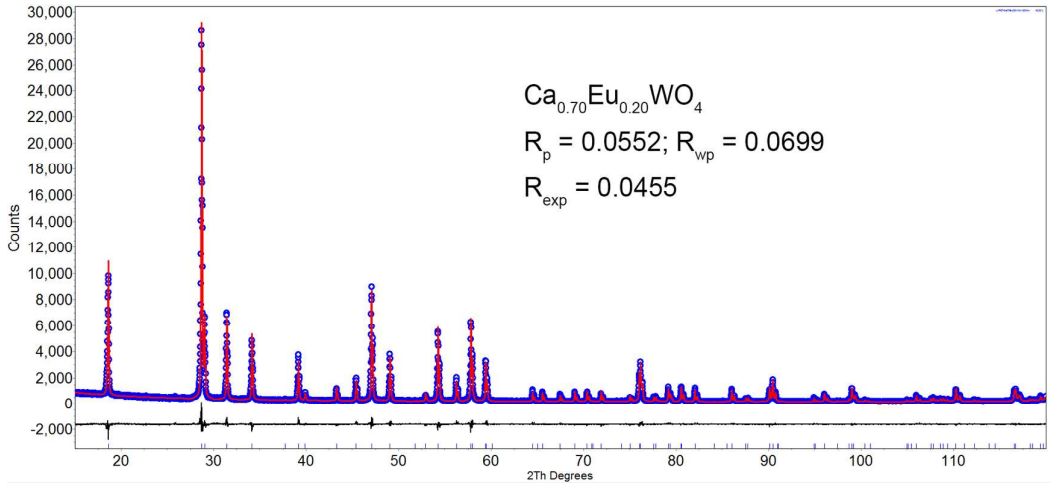

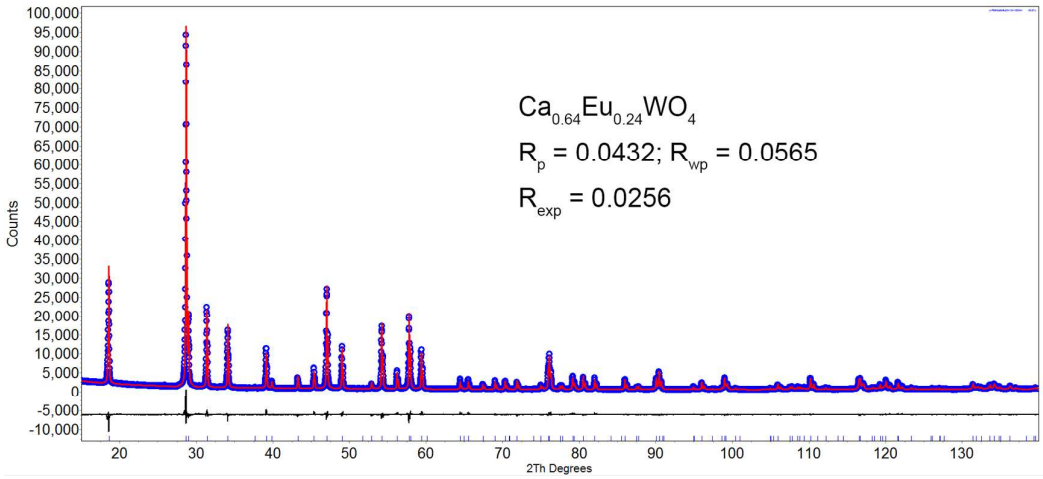

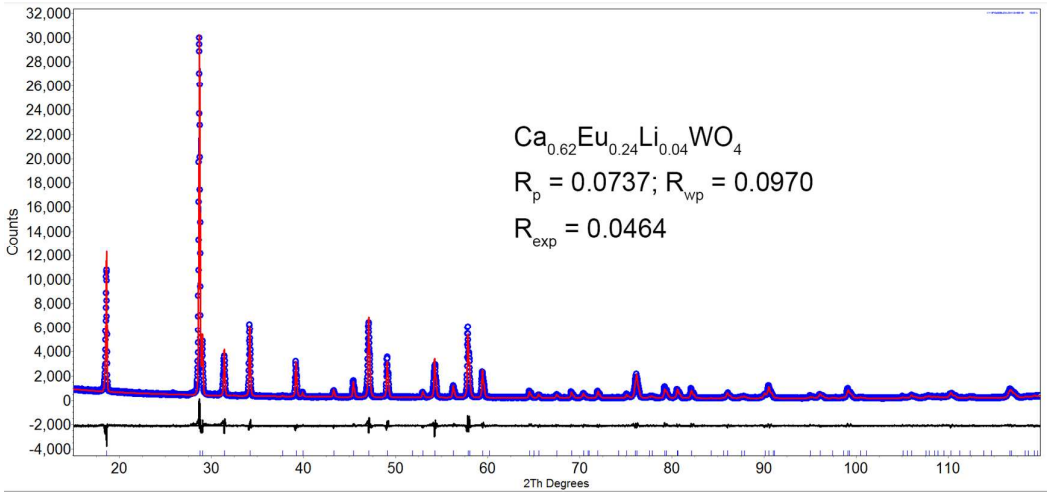

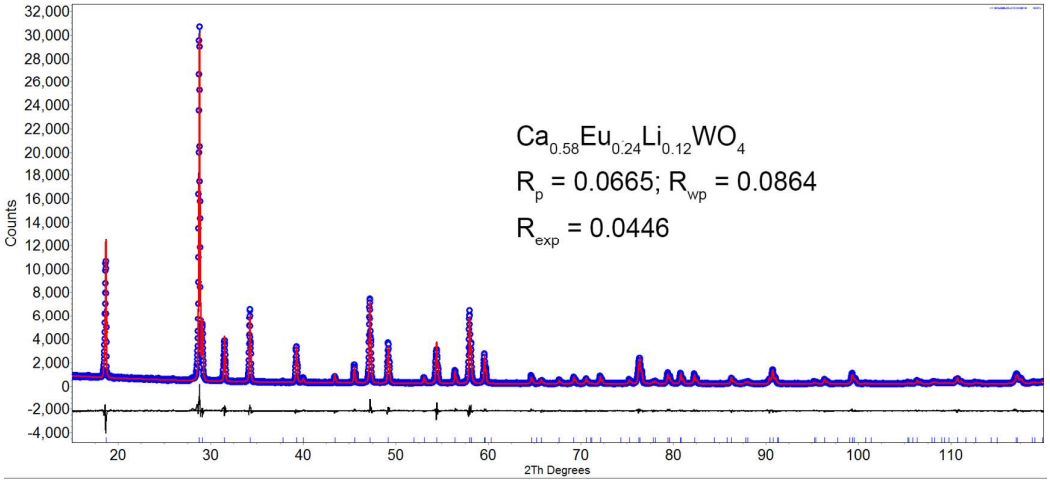

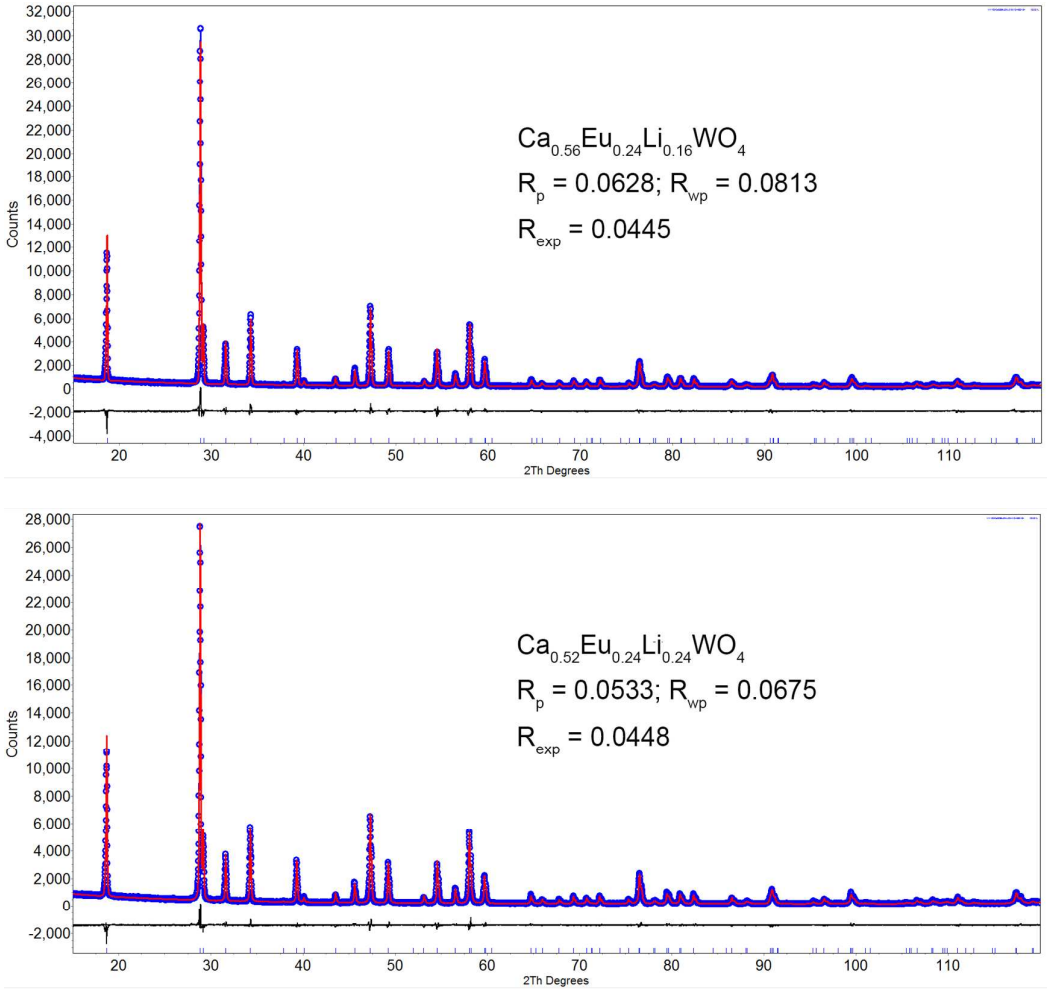

Fig. S4 The final Rietveld refinement patterns of the selected samples for $Sr_{1-1.5x}Eu_x\square_{0.5x}WO_4$ (x = 0.04, 0.12, 0.20, 0.28,0.36), $Sr_{0.64-0.5y}Eu_{0.24}Li_y\square_{0.12-0.5y}WO_4$ (y = 0.04, 0.12, 0.16, 0.24), $Ca_{1-1.5x}Eu_x\square_{0.5x}WO_4$ (x = 0.04, 0.06, 0.12, 0.20,0.24) and $Ca_{0.64-0.5y}Eu_{0.24}Li_y\square_{0.12-0.5y}WO_4$ (y = 0.04, 0.12, 0.16, 0.24). The molecular formula and agreement factors were given in the inserts.

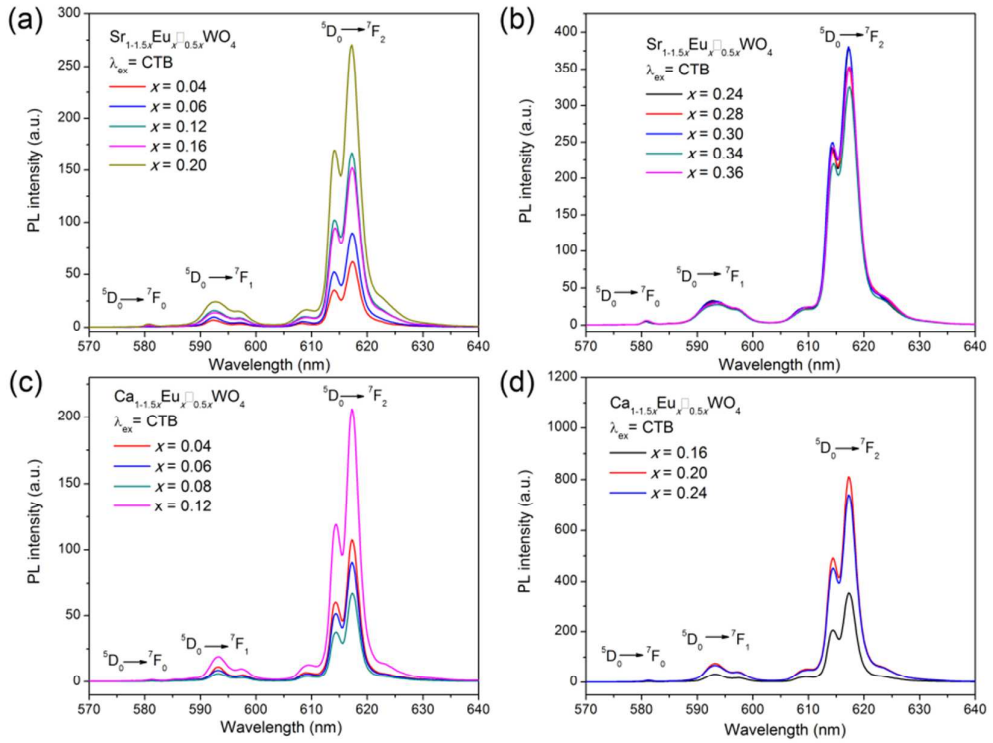

Fig. S5 The emission spectra of **SEW** and **CEW** excited at 274 nm (CT band of $O^{2-} \rightarrow W^{6+}$).

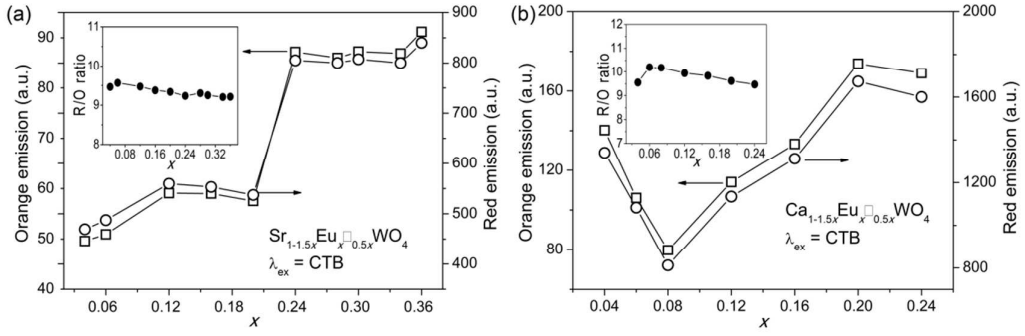

Fig. S6 The emission intensities of (a) **SEW** and (b) **CEW** depend on Eu^{3+} content under 270 nm excitation. The insert of (a) and (b) gives the R/O values.

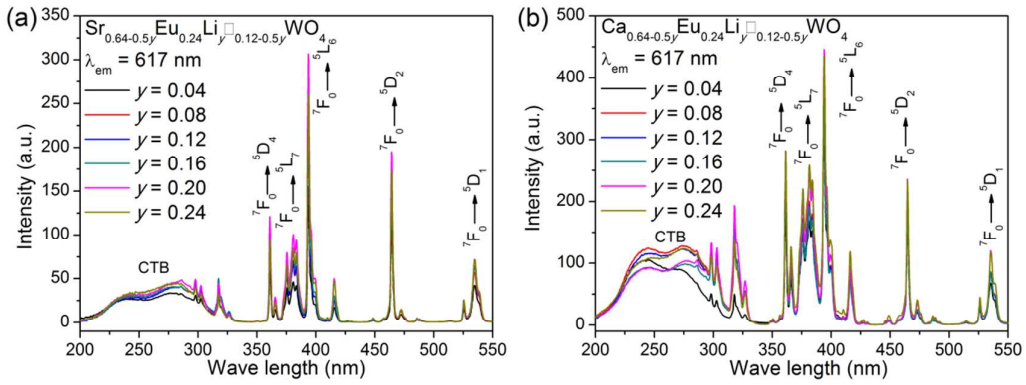

Fig. S7 Excitation spectra of (a) **SELW** and (b) **CELW**, which were measured from 200 to 550 nm by monitoring the strongest emission of Eu^{3+} at 617 nm.

Table S1 The final atomic coordinates, isotropic factors and occupies of the selected samples obtained by Rietveld refinement.

Formula	$Sr_{0.94}Eu_{0.04}WO_4$			$Sr_{0.82}Eu_{0.12}WO_4$		
Atom	Sr/Eu	W	O	Sr/Eu	W	O
x	0	0	0.247(1)	0	0	0.2502(8)
y	0	0	0.1468(8)	0	0	0.1495(7)
z	0.5	0	0.0825(4)	0.5	0	0.0833(4)
Occ.	0.998(3)/0.04	1	1	0.903(3)/0.12	1	1
B_{eq}(Å^2)	0.178(3)	0.010(1)	0.011(3)	0.011(8)	0.006(6)	0.004(1)

Formula	$Sr_{0.70}Eu_{0.20}WO_4$			$Sr_{0.58}Eu_{0.28}WO_4$		
Atom	Sr/Eu	W	O	Sr/Eu	W	O
x	0	0	0.251(1)	0	0	0.256(1)
y	0	0	0.1507(8)	0	0	0.158(2)
z	0.5	0	0.0845(4)	0.5	0	0.0810(6)
Occ.	0.784(4)/0.20	1	1	0.645(5)/0.28	1	1
B_{eq}(Å^2)	0.014(1)	0.007(1)	0.011(3)	0.010(5)	0.003(4)	0.013(6)

Formula	$Sr_{0.46}Eu_{0.36}WO_4$			$Sr_{0.62}Eu_{0.24}Li_{0.04}WO_4$		
Atom	Sr/Eu	W	O	Sr/Eu/Li	W	O
x	0	0	0.248(1)	0	0	0.249(6)
y	0	0	0.153(1)	0	0	0.1459(9)
z	0.5	0	0.0833(4)	0.5	0	0.0844(5)
Occ.	0.575(4)/0.36	1	1	0.672(4)/0.24/0.04	1	1
B_{eq}(Å^2)	0.011(3)	0.005(1)	0.003(3)	0.015(1)	0.0114(8)	0.023(3)

Formula	$Sr_{0.58}Eu_{0.24}Li_{0.12}WO_4$			$Sr_{0.56}Eu_{0.24}Li_{0.16}WO_4$		
Atom	Sr/Eu/Li	W	O	Sr/Eu/Li	W	O
x	0	0	0.2510(9)	0	0	0.2514(9)
y	0	0	0.1450(9)	0	0	0.1490(9)
z	0.5	0	0.0859(4)	0.5	0	0.0859(4)
Occ.	0.586(3)/0.24/0.12	1	1	0.602(3)/0.24/0.16	1	1
B_{eq}(Å^2)	0.0136(9)	0.0140(8)	0.022(2)	0.0147(9)	0.0132(8)	0.019(3)

Formula	$Sr_{0.52}Eu_{0.24}Li_{0.24}WO_4$			$Ca_{0.94}Eu_{0.04}WO_4$		
Atom	Sr/Eu/Li	W	O	Ca/Eu	W	O
x	0	0	0.2549(7)	0	0	0.2557(7)
y	0	0	0.148(1)	0	0	0.1558(7)
z	0.5	0	0.0862(3)	0.5	0	0.0838(3)
Occ.	0.553(2)/0.24/0.24	1	1	1.053(4)/0.04	1	1
B_{eq}(Å^2)	0.0104(6)	0.0121(4)	0.014(1)	0.0175(8)	0.0061(5)	0.009(1)

Formula	$Ca_{0.91}Eu_{0.06}WO_4$			$Ca_{0.82}Eu_{0.12}WO_4$		
Atom	Ca/Eu	W	O	Ca/Eu	W	O
x	0	0	0.2565(7)	0	0	0.2587(8)
y	0	0	0.1570(8)	0	0	0.1561(8)
z	0.5	0	0.0843(3)	0.5	0	0.0846(3
Occ.	0.956(5)/0.06	1	1	0.857(5)/0.12	1	1
B_{eq}(Å^2)	0.0134(8)	0.0055(5)	0.014(1)	0.0132(8)	0.0061(5)	0.013(1)

Formula	$Ca_{0.70}Eu_{0.20}WO_4$			$Ca_{0.64}Eu_{0.24}WO_4$		
Atom	Ca/Eu	W	O	Ca/Eu	W	O
x	0	0	0.2579(8)	0	0	0.2604(7)
y	0	0	0.1615(8)	0	0	0.1639(7)
z	0.5	0	0.0833(4)	0.5	0	0.0828(3)
Occ.	0.753(5)/0.20	1	1	0.720(4)/0.24	1	1
B_{eq}(Å^2)	0.0143(9)	0.0075(8)	0.010(1)	0.0138(5)	0.0056(4)	0.015(1)

Formula	$Ca_{0.62}Eu_{0.24}Li_{0.04}WO_4$			$Ca_{0.58}Eu_{0.24}Li_{0.12}WO_4$		
Atom	Ca/Eu/Li	W	O	Ca/Eu/Li	W	O
x	0	0	0.255(1)	0	0	0.260(1)
y	0	0	0.156(1)	0	0	0.156(1)
z	0.5	0	0.0852(6)	0.5	0	0.0862(5)
Occ.	0.757(7)/0.24/0.04	1	1	0.700(7)/0.24/0.12	1	1
B_{eq}(Å^2)	0.0198(8)	0.0082(5)	0.011(3)	0.0222(9)	0.0119(6)	0.016(3)

Formula	$Ca_{0.56}Eu_{0.24}Li_{0.16}WO_4$			$Ca_{0.52}Eu_{0.24}Li_{0.24}WO_4$		
Atom	Ca/Eu/Li	W	O	Ca/Eu/Li	W	O
x	0	0	0.2572(9)	0	0	0.2555(7)
y	0	0	0.156(1)	0	0	0.1563(8)
z	0.5	0	0.0868(5)	0.5	0	0.0867(4)
Occ.	0.680(6)/0.24/0.16	1	1	0.621(5)/0.24/0.24	1	1
B_{eq}(Å^2)	0.0209(9)	0.0103(5)	0.015(3)	0.0160(9)	0.0055(6)	0.009(1)